Germline mitochondria integrate neuronal cell nonautonomous signaling for the mitochondrial unfolded protein response

Authors: Koning Shen[1], Jenni Durieux[1,2], Cesar G. Mena[1,2], Brant M. Webster[1,4], Kristen Berendzen[5], and Andrew Dillin[1,2,3].

Affiliations:
[1]Department of Molecular & Cellular Biology, University of California, Berkeley, Berkeley CA 94720, USA.
[2]Howard Hughes Medical Institute, University of California, Berkeley, Berkeley CA 94720, USA.
[3]The Helen Wills Neuroscience Institute, University of California, Berkeley, Berkeley CA 94720, USA.
[4]Present affiliation: Denali Therapeutics, South San Francisco, CA 94080, USA.
[5]Weill Institute for Neurosciences, University of California, San Francisco, San Francisco CA 94118, USA.

*Corresponding author: dillin@berkeley.edu

Abstract

The ability of mitochondria to coordinate inter-tissue signaling of stress responses is critical to organismal health and longevity. In *C. elegans*, neurons experiencing mitochondrial stress elicit an inter-tissue signaling pathway that activates the mitochondrial unfolded protein response (UPR^{MT}) in peripheral cells, which promotes organismal health and lifespan. Neurons experiencing mitochondrial stress release mitokine stress signals, such as serotonin or the WNT ligand EGL-20. In peripheral receiving cells, canonical WNT signaling is required to induce the UPR^{MT}. However, a dichotomy exists because the developmental program regulated by WNT signaling is not induced. Therefore, how WNT signaling can be diverged to regulate the UPR^{MT} and not developmental programs is unknown. We find that germline mitochondria play a pivotal role in mediating inter-tissue stress signaling between neurons and the intestine downstream of WNT signaling mechanisms. Through a mutagenesis screen, we identified the mitochondrial complex III subunit *ucr-2.3* as essential for mediating inter-tissue UPR^{MT} signaling. In *C. elegans*, *ucr-2.3* is primarily expressed in neurons and the germline tissue. Surprisingly, we find that only

germline-expressed *ucr-2.3*, not neuronal, mediates cell nonautonomous UPR^{MT} signaling downstream of neuronal factors. Additionally, intact germline tissue was also required for cell nonautonomous UPR^{MT} signaling, suggesting a general role of germline and germline mitochondria for cell nonautonomous mitochondrial stress signaling. Finally, we find that germline mitochondria communicate to the intestine to regulate UPR^{MT} activation through a steroid signaling pathway. Overall, these data propose a model where the germline acts as a central signaling tissue for integrating stress cues from the nervous system to elicit the proper stress responses to maintain organismal integrity. Germline mitochondria, through *ucr-2.3,* may be a key determinant for the cell nonautonomous UPR^{MT} because of the innate role of mitochondria in germline integrity and inter-tissue signaling.

Introduction

Multi-cellular organisms must coordinate the health and function of varied tissues within the organism in order to maintain overall organismal health. This has led to the development of specialized tissues or organs that can communicate long-range signaling with other tissues to ensure organismal health. For instance, the central nervous system regulates the activity of other organs in the body through hormones or neuronal signaling (e.g. neurotransmitters and neuropeptides). Similarly, tissues like muscle or adipose fat can send metabolic or hormonal signals to other components of the body under conditions of hunger, overnutrition, or exercise.

These pathways of inter-tissue signaling become especially crucial during conditions of stress, such as pathogenic infection or cold exposure (Castillo-Armengol et al., 2019; Rao et al., 2017). Inter-tissue signaling pathways are especially relevant in conditions of unhealthy aging, where the aging-induced dysfunction in certain organs may contribute to loss of inter-tissue

communication pathways and a broader loss of organism health (Smith et al., 2020; Van Oosten-Hawle, 2023). Additionally, over-accumulation of inflammation or senescent cells in certain tissues, like muscles and the brain, can release blood-borne factors that affect the aging process (Bieri et al., 2023; Horowitz et al., 2020). In some cases, these secreted factors are protective, such as GDF11 which increases synaptic plasticity and neurogenesis (Bieri et al., 2023; Katsimpardi et al., 2014; Ozek et al., 2018). However, some of these secreted factors aggravate aging, such as the proinflammatory chemokines secreted by senescent cells (Birch and Gil, 2020), suggesting that inter-tissue signaling mechanisms must be tightly regulated to ensure organismal health.

Signals for inter-tissue communication can arise from a multitude of cellular sources, and mitochondria have been shown to be an important source of these signals (Chandel, 2014; Mottis et al., 2019; Shen et al., 2022). This important signaling role for mitochondria may have arisen out of their endosymbiotic origin. When the prokaryotic mitochondrial precursor was engulfed by its now-eukaryotic host, the mitochondria had to develop comprehensive signaling pathways to communicate with its new host cell and nuclear genome. Fittingly, these mitochondrial signaling pathways are highly conserved and have been observed in species ranging from mammals through invertebrates. In particular, mitochondria undergoing dysfunction use inter-tissue signaling pathways to communicate their stress to other tissues and activate protective cellular programs, such as the mitochondrial unfolded protein response (UPR^{MT}), a transcriptional program activated under conditions of mitochondrial stress to alleviate mitochondrial burden and promote overall cellular and organismal health (Houtkooper et al., 2013; Moehle et al., 2019; Shpilka and Haynes, 2018). In mice, low-level mitochondrial stress in POMC neurons induced by *Crif1* heterodeficiency signals to white adipose tissue to increase thermogenesis and activate the UPR^{MT} to protect against obesity and enhance metabolic turnover (Kang et al., 2021). In *Drosophila*,

muscle tissue experiencing mild mitochondrial stress also activates the UPR^{MT} and induces expression of ImpL2 (an ortholog to the human insulin-like growth factor binding protein IGFBP7) that suppresses whole-organism insulin signaling, upregulates mitophagy, and promotes longevity and muscle function (Owusu-Ansah et al., 2013).

Much of the mechanistic work investigating inter-tissue mitochondrial signaling has been performed in *C. elegans* using a model of inter-tissue (or cell nonautonomous) communication of the UPR^{MT} between neurons and the intestine (Durieux et al., 2011). In this model, neurons experiencing mitochondrial stress, such as neuron-specific knockdown of mitochondrial genes (Durieux et al., 2011), expression of the aggregation-prone mutant PolyQ40 protein, or neuron-specific targeting of KillerRed to mitochondria (Berendzen et al., 2016), activate the UPR^{MT} in the intestine, a tissue in *C. elegans* completely peripheral and non-innervated by neurons **(Fig 1A)**. Intestinal activation of UPR^{MT} by these neurons protected organismal health, as inhibition of UPR^{MT} activation decreased organismal fitness in the presence of neuronal mitochondrial stress (Berendzen et al., 2016).

Several neuronal factors mediating neuron-to-intestine UPR^{MT} signaling in *C. elegans* have been identified. Neuron-specific over-expression of the histone demethylases *jmjd-1.2* and *jmjd-3.1* induces intestinal UPR^{MT} even in the absence of mitochondrial stress and also regulates activation of UPR^{MT} in mice (Merkwirth et al., 2016). Neuronal release of neurotransmitters, serotonin, or the neuropeptides FLP-1 and FLP-2 are also critical in mediating cell nonautonomous activation of the UPR^{MT} in the intestine (Berendzen et al., 2016; Jia and Sieburth, 2021; Shao et al., 2016). The WNT ligand, EGL-20, was identified as a bona fide "mitokine" as it is both necessary and sufficient for activation of the intestinal UPR^{MT} upon neuron-specific over-expression (Zhang et al., 2018). Furthermore, neuronal release of the EGL-20 WNT ligand

engaged canonical WNT signaling pathway in the peripheral intestinal cells to activate the UPR^{MT} (Zhang et al., 2018). However, it is unclear how this WNT signaling, in the context of neuronal mitochondrial stress, could specifically induce the UPR^{MT} and not its canonical developmental programs in the intestine.

To address this question, we performed a genome-wide mutagenesis screen to identify molecular players that mediated UPR^{MT} cell nonautonomous signaling between neurons and the intestine. Through this screen, we identified mutations in *ucr-2.3* that are essential in mediating cell nonautonomous UPR^{MT} signaling between neurons and the intestine. *ucr-2.3* is a mitochondrial electron complex III gene, homologous to mammalian UQCRC2, and is expressed primarily in a few neurons and the germline of *C. elegans*. Surprisingly, we discovered that germline activity, not neuronal, of *ucr-2.3* mediates the cell non-autonomous UPR^{MT} signaling between the neurons and intestine. In addition, the germline plays a general role in mediating cell nonautonomous UPR^{MT} signaling, as loss of the germline through either genetic or pharmacological treatments abolishes neuron-to-intestine UPR^{MT} activation, but not other neuronal derived stress signals. These data suggest that integrity of the germline tissue, mediated through germline UCR-2.3 mitochondrial activity, is integral for neuron-to-intestinal signaling of the UPR^{MT}. Finally, we find that germline integrity may regulate intestinal UPR^{MT} activation through a steroid hormone signaling pathway mediated by DAF-9, a cytochrome P450 enzyme that synthesizes steroid hormones, that controls lipid levels in the intestine. Overall, our work showcases a signaling role for the germline, once thought of as a tissue insulated from the soma, in directly communicating with somatic tissues for stress signaling. Additionally, our results provide broader implications for the importance of germline mitochondrial quality and its

consequences on steroid hormone signaling, lipid metabolism, and the consequences of these interactions on organismal stress signaling and fertility.

Results

Mutagenesis screen reveals the requirement of *ucr-2.3* in neuronal UPR^{MT} signaling

To identify novel regulators of inter-tissue (or cell nonautonomous) mitochondrial signaling in *C. elegans*, we conducted a genome-wide mutagenesis screen using a genetic model where neurons expressing an aggregation-prone mutant PolyQ40 protein tagged with YFP (*rgef-1p::Q40::*YFP) activate the mitochondrial unfolded protein response (UPR^{MT}) in the intestine (Berendzen et al., 2016) **(Fig 1A)**. Activation of the UPR^{MT} in the intestine can be assessed by a transcriptional reporter for expression of *hsp-6*, the mitochondrial Hsp70 chaperone induced by activation of the UPR^{MT} (Shpilka and Haynes, 2018) **(Fig 1A)**. After identifying mutants with suppressed intestinal UPR^{MT} but intact neuronal PolyQ40 signal, we used SNP mapping and whole genome sequencing approaches (Doitsidou et al., 2010) to identify a missense mutation in the gene *ucr-2.3* that suppressed cell nonautonomous UPR^{MT} signaling **(Supp Fig 1A, F)**. We independently verified the necessity of *ucr-2.3* in mediating cell nonautonomous UPR^{MT} signaling by creating several alleles of early stop nonsense-mediated decay (NMD) mutations in *ucr-2.3* through CRISPR/Cas9 genome editing and verified that they all suppressed PolyQ40-mediated cell nonautonomous UPR^{MT} **(Fig 1B; Supp Fig 1B, F)**. Importantly, the NMD early stop mutation in the *ucr-2.3(uth252)* allele leads to almost complete loss of gene expression, thus effectively creating a null allele **(Supp Fig 1D, F)**. We also tested a *ucr-2.3* mutant containing a large deletion spanning exons 3-4 resulting in an early termination codon and found that it also suppressed cell nonautonomous UPR^{MT} signaling **(Supp Fig 1C, F).** We next tested whether *ucr-2.3* was involved

in other models of cell nonautonomous UPR^{MT} signaling, such as neuron-specific knockdown of the mitochondrial complex IV subunit *cco-1* (*rab-3p::cco-1* hairpin in the *sid-1(qt9)* genetic background), which also activates UPR^{MT} in the intestine (Durieux et al., 2011). We find that a null mutation in *ucr-2.3* also suppresses this model of cell nonautonomous UPR^{MT} signaling **(Fig 1C)**. We conclude that *ucr-2.3* is as a novel regulator of neuron-to-intestine UPR^{MT} signaling induced by multiple forms of neuronal mitochondrial stress.

Next, we tested whether *ucr-2.3* was required for cell autonomous induction of the UPR^{MT}. We tested this by feeding *cco-1* RNAi targeting a mitochondrial complex IV subunit to wildtype and *ucr-2.3* mutant strains to ask whether loss of *ucr-2.3* impairs cell-autonomous activation of the UPR^{MT}. We find that *ucr-2.3* loss of function mutants activate the UPR^{MT} cell autonomously, with and without neuronal PolyQ40 expression **(Fig 1D, Supp Fig 1E)**. These data indicate that the *ucr-2.3* is not involved in general machinery of UPR^{MT} activation but rather has a specific role in cell nonautonomous signaling of mitochondrial stress. We also find that loss of *ucr-2.3* non-autonomous UPR^{MT} signaling is not a temporary delay. Rather, the suppression of non-autonomous UPR^{MT} signaling by the *ucr-2.3* mutation increases over aging **(Supp Fig 1G)**. Finally, we tested the specificity in *ucr-2.3* loss in nonautonomous stress signaling and find that *ucr-2.3* loss of function does not suppress cell nonautonomous signaling of the UPR^{ER} or the cytosolic stress response between neurons and the intestine **(Supp Fig 2A-B)**. Conversely, there is a slight up-regulation of both stress responses upon *ucr-2.3* loss of function. Overall, our data indicate that *ucr-2.3* is a critical and specific gene required for mediating cell nonautonomous UPR^{MT} signaling between neurons and the intestine in *C. elegans*.

UCR-2.3 is a mitochondrial protein with a novel role in mitochondrial stress signaling

The *ucr-2.3* gene encodes UCR-2.3 in *C. elegans*, which is reported to be a mitochondrial protein homologous to mammalian UQCRC2, a core subunit of respiratory complex III of the electron transport chain (Iwata et al., 1998; Nomura et al., 2006). That the loss of *ucr-2.3* function results in a loss of UPR^{MT} neuronal signaling was perplexing, as the knockdown of many mitochondrial proteins, especially those involved in the electron transport chain, activate, not suppress, the UPR^{MT} (Durieux et al., 2011; Houtkooper et al., 2013; Nargund et al., 2012).

We experimentally confirmed that the UCR-2.3 protein is a mitochondrial protein using three orthogonal approaches. First, we performed a sub-cellular fractionation in *C. elegans* expressing *ucr-2.3* with an HA epitope endogenously inserted at the *ucr-2.3* genomic locus using CRISPR/Cas9 editing **(Fig 2A*i*)**. Compared to the cytosolic fraction, we detect enrichment of UCR-2.3 in the mitochondrial fraction, similar to NDUFS3, a subunit of mitochondrial electron transport complex I **(Fig 2A*ii*)**. This is opposed to α-tubulin, which was detected predominantly in the cytosolic fraction. Second, using human RPE-1 human cells, we over-expressed the *C. elegans* UCR-2.3 protein tagged with mNeonGreen alongside an outer mitochondrial membrane protein OMP25 tagged with BFP. We find that UCR-2.3 and OMP-25 thoroughly co-localize, indicating the UCR-2.3 is localized to mitochondria **(Fig 2B)**. Indeed, upon closer examination, we observe that UCR-2.3 primarily localizes within the OMP25 signal, suggesting that UCR-2.3 is located within the mitochondrial matrix, consistent with its purported role as a matrix-facing core subunit of complex III like UQCRC2 **(Fig 2B*ii*)** (Iwata et al., 1998). Third, we observed that UCR-2.3 functionally acted as a mitochondrial protein. Using the null mutation in *ucr-2.3* in *C. elegans*, we observed that loss of *ucr-2.3* decreased mitochondrial respiration **(Fig 2C)**. Thus, we conclude that *ucr-2.3* encodes a bona fide mitochondrial protein in *C. elegans*, which has a similar sub-cellular localization and function to its mammalian ortholog UQCRC2.

Next, we tested whether UCR-2.3 mitochondrial localization was essential for its role in mediating cell nonautonomous UPR^{MT} signaling. Using CRISPR/Cas9 genomic editing, we excised the predicted mitochondrial targeting sequence (MTS) of UCR-2.3 predicted by MitoFates (Fukasawa et al., 2015) from UCR-2.3 and found that this mutant *ucr-2.3(ΔMTS)* had suppressed intestinal UPR^{MT} signaling **(Fig 2D)**. We confirmed that deletion of the MTS had no effect on expression of the *ucr-2.3* mutant construct **(Supp Fig 2C)**. Overall, from these results, we conclude that *ucr-2.3* encodes a mitochondrial localized protein whose mitochondrial activity is important for mediating neuron-to-intestine cell nonautonomous UPR^{MT} signaling.

ucr-2.3* has a unique role within the UCR-2 gene family in *C. elegans

ucr-2.3 belongs to a family of paralogs in the UCR-2 family in *C. elegans* that are all homologous to mammalian UQCRC2: *ucr-2.1, ucr-2.2,* and *ucr-2.3* **(Fig 3A)** (Howe et al., 2016). To investigate whether the other paralogs of the UCR-2 family were similarly involved in cell nonautonomous UPR^{MT} signaling, we made similar early-termination NMD mutations in *ucr-2.1* and *ucr-2.2* using CRISPR/Cas9 editing **(Supp Fig 3E*i-ii*)**. Surprisingly, we found that only genetic loss of *ucr-2.3* suppressed cell nonautonomous UPR^{MT} signaling; genetic loss of *ucr-2.1* or *ucr-2.2* slightly activated, not suppressed, UPR^{MT}, more in alignment with the expectation of a canonical mitochondrial gene knockdown **(Fig 3B)**. This suggested that *ucr-2.3* has a unique role among the UCR-2 family genes, whereas *ucr-2.1* and *ucr-2.2* may be more similar.

Next, we next sought to explore the functional and genetic relationships among the UCR-2 family genes. First, we observed that *ucr-2.1* and *ucr-2.2* were functionally redundant with each other with respect to their role in the mitochondrial electron transport chain, but neither were redundant with *ucr-2.3.* While knockdown of *ucr-2.3* reduced mitochondrial respiration **(Fig 2C)**,

only the double knockdown of *ucr-2.1* and *ucr-2.2* reduced mitochondrial respiration **(Supp Fig 3A)**. Individual knockdown of either *ucr-2.1* or *ucr-2.2* had no effect on respiration, suggesting that these two genes are functionally redundant with each other **(Supp Fig 3A)**. In addition, double knockdown of *ucr-2.1* and *ucr-2.2* strongly activated UPR^{MT} **(Supp Fig 3B)**. As this strong activation is consistent with the expectation of a canonical mitochondrial ETC gene knockdown (Durieux et al., 2011; Houtkooper et al., 2013), this provides further evidence that *ucr-2.1* and *ucr-2.2* are functionally redundant with each other for a role in the mitochondrial electron transport chain. In contrast, we observed that double knockdown of either *ucr-2.1* and *ucr-2.3* or *ucr-2.2* and *ucr-2.3* could not activate UPR^{MT}; only conditions in which both *ucr-2.1* and *ucr-2.2* are knocked down could UPR^{MT} be activated **(Supp Fig 3C)**. This finding further suggests that neither *ucr-2.1* nor *ucr-2.2* are functionally redundant with *ucr-2.3.* In addition, we analyzed how knockdown of these UCR-2 family genes affected each other transcriptionally. We found that while knockdown of *ucr-2.3* increased expression of *ucr-2.1* and *ucr-2.2* **(Supp Fig 3D)**, knockdown of either *ucr-2.1* or *ucr-2.2* individually or together had no effect on *ucr-2.3* expression **(Supp Fig 3E)**. One interpretation of this result is that loss of *ucr-2.3* function requires compensation from both *ucr-2.1* and *ucr-2.2* equally, while loss of either *ucr-2.1* or *ucr-2.2* does not require *ucr-2.3.* Overall, these data suggest that *ucr-2.1* and *ucr-2.2* are functionally redundant with each other while *ucr-2.3* may have an independent role.

Most importantly, we found that the UCR-2 family genes differ in their tissue expression patterns **(Fig 3C-D)**. Using genomic, tissue-specific, and single cell transcriptomic databases, we found that while *ucr-2.1* and *ucr-2.2* expression is mostly ubiquitous through the animal, *ucr-2.3* expression is enriched in the germline and neuronal cells (Cao et al., 2017; Howe et al., 2016; Kaletsky et al., 2018) **(Supp Fig 3F)**. We confirmed these reports by generating an endogenous

transcriptional expression reporter system for each of the UCR-2 genes by inserting an mCherry::F2A construct between the promoters of *ucr-2.1*, *ucr-2.2*, and *ucr-2.3* and the respective CDS at the endogenous genomic loci using CRISPR/Cas9 editing **(Fig 3C)**. The tissue expression patterns confirm that *ucr-2.1* and *ucr-2.2* are ubiquitously expressed throughout the animal. Interestingly, *ucr-2.1* and *ucr-2.2* were excluded from the germline **(Fig 3C*i-ii*, 3D)**. In contrast, *ucr-2.3* expression was exclusively localized to the germline as well as a few cells in the head of the animal **(Fig 3C*iii*, 3D)**. To determine which of these head cells expressed *ucr-2.3*, we crossed the *ucr-2.3* expression reporter strain to an *rgef-1p::GFP* construct driving GFP expression in neurons and found that the pattern of *ucr-2.3* expression mostly overlapped with the GFP signal **(Fig 3E)**, suggesting that the cells expressing *ucr-2.3* are indeed neurons. In summary, our data indicate that *ucr-2.3* differs starkly in its tissue expression from *ucr-2.1* and *ucr-2.2*, which may explain the unique role of *ucr-2.3* in mediating cell nonautonomous UPR^{MT} signaling.

The germline role of *ucr-2.3* is critical for mediating nonautonomous UPR^{MT}

We were intrigued by the tissue-specific expression patterns of *ucr-2.3* and wondered whether this tissue-specific nature conferred the ability of *ucr-2.3* to mediate cell nonautonomous UPR^{MT} signaling. To answer this, we sought to determine the site of action for *ucr-2.3* for its role in cell nonautonomous UPR^{MT} signaling. We designed a tissue-specific rescue experiment using the single copy mosSCI system (Frøkjær-Jensen et al., 2008) **(Fig 4A)**. Briefly, we knocked in an integrated wildtype copy of *ucr-2.3* driven by a tissue-specific promoter into a mutant strain of *ucr-2.3*. As we observed that *ucr-2.3* is expressed in neuronal cells and the germline **(Fig 3C-D)**, we tested whether either neuronal or germline-specific expression of wildtype *ucr-2.3* could rescue cell nonautonomous UPR^{MT} signaling in the *ucr-2.3* mutant, using the neuron-specific promoter

rgef-1 and the germline-specific promoter *pie-1* **(Fig 4A)**. We found that expression of a wildtype copy of *ucr-2.3* driven by the germline-specific promoter *pie-1* could completely rescue the cell nonautonomous UPR^{MT} signal suppressed by loss of *ucr-2.3*, whereas *rgef-1p* neuronal-driven expression of *ucr-2.3* had no appreciable effect on cell nonautonomous UPR^{MT} signal **(Fig 4B)**. In addition, one of our initial observations of the *ucr-2.3* mutants were that they had reduced brood size (number of progeny) **(Fig 4C)**. We found that germline rescue of *ucr-2.3* could also completely restore the brood size phenotype we observed with *ucr-2.3* mutants, whereas neuronal rescue of *ucr-2.3* had no effect on the brood size **(Fig 4C)**.

We also used the FLP/FRT recombinase system to test how a neuron-specific knockout of *ucr-2.3* affected nonautonomous UPR^{MT} signaling (Muñoz-Jiménez et al., 2017). We were unable to use this system to test germline-specific knockout because germline-specific FLP/FRT recombination becomes pervasive in all tissues in the following generation (Macías-León and Askjaer, 2018). To design a neuron-specific FLP/FRT recombinase knockout system, we used the *rgef-1p* neuronal promoter to drive FLP recombinase and inserted FRT sites in the introns of *ucr-2.3* at the genomic locus. In this way, FLP recombination of *ucr-2.3* induced a large deletion in the *ucr-2.3* genomic locus only in neuronal cells, which we confirmed by PCR genotyping **(Supp Fig 4A*iii*)**. While *ucr-2.3* containing FRT sites had slightly reduced cell nonautonomous UPR^{MT} signal, we find that FLP induced recombination of *ucr-2.3* did not enhance reduction of the cell nonautonomous UPR^{MT} signal and did not phenocopy the loss of function *ucr-2.3* genetic mutant **(Supp Fig 4A*i-ii*)**. Overall, these data identify that *ucr-2.3* mediates cell nonautonomous UPR^{MT} signaling through its activity in the germline tissue.

Having previously discovered a role for *ucr-2.3* in mitochondrial respiration **(Fig 2C)**, we next asked how much of *ucr-2.3* mitochondrial activity is confined to the germline tissue. We

tested this by using a *C. elegans* strain with a temperature sensitive mutation in the *glp-4* gene, which arrests germ cell proliferation at the restrictive temperature 25 °C to create germline deficient adult animals (Beanan and Strome, 1992). We find that at even at the restrictive temperature 25 °C, *ucr-2.*3 loss of function still decreases mitochondrial respiration **(Fig 4D)**. Germline deficient animals also have decreased mitochondrial respiration, likely due to the loss of the high population of mitochondria in the germline **(Fig 4D)** (Tsang and Lemire, 2002). However, additional loss of *ucr-2.3* function in the germline deficient animals has no impact on mitochondrial oxygen consumption **(Fig 4D)**. In contrast, feeding germline deficient animals with a RNAi targeting the *cco-1* complex IV subunit could further decrease mitochondrial respiration **(Fig 4D)**. This indicates that the vast majority of *ucr-2.3* contribution to mitochondrial respiration is in the germline.

In addition, we find that loss of *ucr-2.3* greatly changes morphology and content of germline mitochondria. Using a germline-specific mitochondrial morphology reporter strain (Ahier et al., 2018), we observe that wildtype animals have a dense network of mitochondria throughout the germline tissue **(Fig 4E)**. However, the *ucr-2.3* mutation results in a more punctate and sparser mitochondrial network in the distal germ cells and especially oocytes **(Fig 4E)**. This suggests that loss of *ucr-2.3* directly affects quality of germline mitochondria, and that loss of this germline mitochondrial quality may compromise cell nonautonomous UPR^{MT} signaling.

ucr-2.3 mediates cell nonautonomous UPR^{MT} downstream of established neuronal factors in UPR^{MT} signaling

By identifying the critical role of germline *ucr-2.3* in mediating UPR^{MT} signaling between neurons and the intestine, we then asked whether germline *ucr-2.3* functioned downstream of

previously identified neuronal signaling factors (Berendzen et al., 2016; Merkwirth et al., 2016; Zhang et al., 2018). For instance, neuronal overexpression of the WNT ligand *egl-20* and the histone demethylase *jmjd-1.2* can activate intestinal UPR^{MT} even in the absence of neuronal mitochondrial stress **(Fig 5A)** (Merkwirth et al., 2016; Zhang et al., 2018). We find that loss of *ucr-2.3* suppressed intestinal UPR^{MT} activation even in the presence of neuronal over-expression of *egl-20* and *jmjd-1.2* **(Fig 5B-C)**. This brings further evidence placing the working role of *ucr-2.3* in the germline downstream of these neuronal factors to mediate cell non-autonomous UPR^{MT} signaling. Additionally, we find that germline RNAi-specific knockdown of UPR^{MT} regulators, such as *atfs-1*, *egl-20*, and *jmjd-1.2,* do not suppress cell non-autonomous UPR^{MT} signaling **(Supp Fig 5A)**, suggesting that the germline has an independent role from these other neuronal factors for mediating cell nonautonomous UPR^{MT}.

One of the factors we considered that could signal to the germline was serotonin, a neurotransmitter that is released by dense core vesicles and mediates cell nonautonomous activation of intestinal UPR^{MT} upon neuronal mitochondrial stress (Berendzen et al., 2016). We directly tested whether *ucr-2.3* acted downstream of serotonin signaling by testing whether exogenous serotonin addition could rescue cell nonautonomous UPR^{MT} signaling between neurons and the intestine. While we found that exogenous addition of serotonin (5-HT) could increase intestinal UPR^{MT} signaling in the wildtype animal, while loss of function in *ucr-2.3* prevented serotonin-mediated activation of intestinal UPR^{MT} **(Fig 5D)**. Therefore, *ucr-2.3* functions not only downstream of *egl-20* and *jmjd-1.2*, but also downstream of serotonin signaling pathways to mediate intestinal UPR^{MT} activation upon neuronal mitochondrial stress.

The germline, and germline mitochondria, is required for cell nonautonomous UPR^{MT} signaling

Given the essential role of *ucr-2.3* in the germline, we simply asked if general germline function or germline mitochondria were also essential for mediating cell nonautonomous UPR^{MT} signaling. We tested this using genetic and pharmacological methods to deplete the germline in *C. elegans*. For genetics, we generated germline deficient animals using two temperature sensitive mutations *glp-4(bn2)* and *glp-1(e2141ts)*, which both restrict germ cell proliferation at the restrictive temperature of 25 °C (Beanan and Strome, 1992; Mello et al., 1994). We then asked whether germline deficient animals also have suppressed the cell nonautonomous UPR^{MT} signaling. Indeed, we observed that germline deficient animals through the *glp-1* and *glp-4* temperature sensitive mutations suppress cell nonautonomous UPR^{MT} signaling in the neuronal PolyQ40 stress model **(Fig 6A*i-ii*)**. Interestingly, the *glp-1(e2141ts)* allele is long-lived while *glp-4(bn2)* is not (Greer et al., 2010; TeKippe and Aballay, 2010), decoupling germline-mediated suppression of UPR^{MT} signaling from longevity mechanisms. In addition, we find that the *glp-4(bn2)* restrictive mutation also suppresses cell nonautonomous UPR^{MT} signaling for the neuron-specific *cco-1* knockdown model **(Fig 6A*iii*)**. For a pharmacological method, we used the drug FUDR to ablate the germline through prohibiting DNA replication, especially of mitochondria in the developing germline (Tsang and Lemire, 2002) **(Fig 6B)**. We found that FUDR treatment depleted the germline of mitochondria **(Supp Fig 5B)** as well as suppressed cell nonautonomous activation the UPR^{MT} in both the neuronal PolyQ40 and *cco-1* RNAi hairpin models **(Fig 6B)**. Together, these data demonstrate that an intact germline is essential for cell nonautonomous UPR^{MT} signaling.

We also tested the specificity of the germline in regulating cell nonautonomous stress response signaling, like for the UPR^{ER} or HSR. We find that FUDR treatment did not appreciably

inhibit UPR^{ER} cell nonautonomous signaling in the UPR^{ER}, although it did decrease the HSR model **(Supp Fig 5C)**. We observed that the FUDR-treated HSR model animals were small and sick, so the lack of HSR signal may result from additional drug interactions with FUDR treatment. We also tested whether genetic germline depletion via the *glp-4(bn2)* temperature sensitive mutation also impacted cell nonautonomous signaling in the UPR^{ER} or HSR models. While we found the signaling models to be more variable at the 25 °C restrictive temperature, we did not see appreciable reduction in cell nonautonomous signaling like for the UPR^{MT} **(Supp Fig 5D)**. Overall, these results suggest that depletion of the germline tissue or germline mitochondria specifically inhibits cell nonautonomous UPR^{MT} stress signaling between neurons and the intestine.

The germline may communicate via steroid hormone signaling pathway to regulate UPR^{MT} activation and lipid levels in the intestine

Although our data indicate the *ucr-2.3* works downstream of the neuronal factors in regulating intestinal UPR^{MT} activation, our data do not rule out the possibility that *ucr-2.3* works in parallel with the neuronal factors to coordinate UPR^{MT} induction in peripheral cell types. In this scenario, a signal might be sent from the germline to work with WNT signaling in peripheral cells like the intestine to specifically induce the UPR^{MT} and not developmental programs mediated by canonical WNT signaling.

To identify what signals could be sent from the germline to regulate UPR^{MT} induction in the intestine, we considered existing models between germline mitochondria and the intestine, such as through lipid or lipophilic/steroid hormone signaling (Berman and Kenyon, 2006; Han et al., 2017; Wang et al., 2008). We were particularly motivated to explore a lipid-based germline signaling model for several reasons. One of our initial observations of the *ucr-2.3* mutant was that

it had drastically higher levels of intestinal fat **(Fig 7A, Supp Fig 6A)**. Additionally, we were intrigued by a report that germline-to-intestinal stress signaling could occur via the *daf-9* steroid signaling pathway (Berman and Kenyon, 2006). In this pathway, the reproductive system communicates to the intestine via a steroid hormone synthesized by the cytochrome P450 enzyme *daf-9*. Since mitochondria are also major sites for steroid hormone synthesis (Miller, 2013), we wanted to ask whether a steroid hormone signaling pathway would also be relevant in germline-to-intestinal communication in the *ucr-2.3* mutant animals with compromised germline mitochondria. We tested this by combining the *daf-9(rh50)* hypomorphic allele with the *ucr-2.3* loss of function and found that the *daf-9* loss of function could rescue intestinal UPR^{MT} signal in the *ucr-2.3(uth252)* mutant background **(Fig 7B).** In addition, we find that the *daf-9* mutant animals decrease intestinal fat levels in the *ucr-2.3* mutant animals **(Fig 7C)**, suggesting that *daf-9* steroid hormone signaling may regulate intestinal UPR^{MT} activation through modulating lipid levels in the intestine. Indeed, previous work had shown that mitochondrial stress signaling can be regulated by various lipids, such as ceramides and cardiolipins (Kim et al., 2016), raising the possibility that intestinal lipid levels – controlled by the integrity of the germline tissue and *daf-9* signaling – could regulate intestinal UPR^{MT} activation.

Collectively our data propose a model in which the germline, through germline mitochondrial activity, acts as a signaling tissue to integrate signaling from the nervous system for regulating UPR^{MT} in peripheral tissues, such as the intestine **(Fig 7D)**. Our data highlight a new role of the germline tissue as actively communicating mitochondrial stress with somatic tissues. We believe the evolutionary basis for this somatic-to-germline signaling circuit may be to conserve overall organismal resources. The need to activate energy-intensive protective stress responses should only be executed in the presence of a functioning germline, to preserve progeny production

and continuation of the species. On a broader level, we believe this signaling circuit has implications for how germ cells and germline mitochondrial quality may be influenced by stresses occurring in the somatic environment, such as with aging, metabolic disease, or infection.

Discussion

In this study, we have identified the importance of the germline, and particularly of germline mitochondria, in mediating cell nonautonomous communication of mitochondrial stress. Using a genome-wide mutagenesis screen, we identified a mitochondrial gene *ucr-2.3* as a novel regulator of cell nonautonomous UPR^{MT} signaling between neurons and the intestine in *C. elegans*. Surprisingly, we find that *ucr-2.3* mediates cell nonautonomous UPR^{MT} signaling through its activity in the germline tissue. Loss of *ucr-2.3* activity in the germline compromises germline mitochondrial health, germline integrity, and suppresses neuronal-to-intestinal communication of mitochondrial stress signals. Furthermore, we find that *ucr-2.3* works downstream and independently of other identified neuronal mediators of cell nonautonomous UPR^{MT} signaling such as serotonin and *egl-20*/WNT mechanisms. We also observe that *ucr-2.3* and germline tissue integrity is specific to UPR^{MT} cell nonautonomous signaling and is not a primary mediator for other forms of cell nonautonomous communication, such as the UPR^{ER} or cytosolic HSR. This suggests that there is a specific relationship between germline mitochondrial integrity and coordination of inter-tissue mitochondrial stress responses in the somatic tissues. Finally, we find that *ucr-2.3* activity in the germline may communicate to the intestine through a steroid hormone signaling pathway that may work downstream of *ucr-2.3* activity in the germline to control fat storage levels in the intestine and regulate UPR^{MT} activation. We propose that this germline-to-intestine signal could also direct WNT signaling factors from their role in developmental programs

to regulating UPR^{MT} activation (Zhang et al., 2018). Overall, our data highlight the role of germline tissue in mediating cell nonautonomous mitochondrial stress signaling. That the germline's ability to coordinate this signaling may be dictated by germline mitochondria quality suggests a possible role for germline mitochondria in the general coordination of inter-tissue stress signaling.

Our findings suggest two models for how the germline could mediate neuronal-to-intestinal UPR^{MT} signaling **(Fig 7D)**. In one model ("Parallel Signaling"), the germline acts as an ON/OFF switch for intestinal UPR^{MT} activation. In this case the absence of an intact germline would prohibit activation of intestinal UPR^{MT} activation even in the presence of a neuronal stress stimulus, such as EGL-20 or serotonin. In another model ("Direct Signaling"), the germline could act as an intermediary tissue, wherein the germline receives signals secreted by neurons experiencing mitochondrial stress, processes these signals – perhaps through mitochondrial *ucr-2.3* activity – then emits an additional signal to the intestine to regulate UPR^{MT} activation. In both models, the germline may regulate intestinal activation of UPR^{MT} signaling through steroid hormone signaling and intestinal fat storage levels.

Based on our findings, we cannot disprove either the Parallel or Direct Signaling model nor have we shown direct evidence that germline mitochondria can receive signals from neurons. However, regarding the possibility of a Direct Signaling model, we do observe that germline mitochondrial activity works downstream of serotonin signals **(Fig 5D)**. In addition, it had been previously shown that in the same neuronal polyQ40 model of mitochondrial stress in *C. elegans*, neuronal mitochondrial stress elevated mtDNA levels in germline mitochondria, which could be transgenerationally inherited (Q. Zhang et al., 2021). Furthermore, components of the WNT signaling pathway, such as the beta-catenin *bar-1,* were also shown to directly regulate oocyte mitochondria mass and mtDNA levels (Q. Zhang et al., 2021). Serotonin signaling has also been

shown to directly improve oocyte quality in *C. elegans* and *D. melanogaster* (Aprison et al., 2023), suggesting that a Direct Signaling route between neurons and germ tissue through serotonin-based signaling could exist.

The mechanism for how *ucr-2.3* activity in the germline controls cell nonautonomous UPR^{MT} remains to be explored. One possibility is that loss of *ucr-2.3* function leads to compromised mitochondrial function in the germ cells **(Fig 2C, Fig 4D, Supp Fig 5B)**, leading to a general depletion of germ cell proliferation and resulting germline tissue. This is reflected in the very small brood size of *ucr-2.3* mutant animals **(Fig 4C)**. In this scenario, the loss of functional *ucr-2.3* compromises general germline integrity, leading to a loss of cell nonautonomous signaling. Indeed, we believe the germline-specific expression of *ucr-2.3* is why only mutations in *ucr-2.3* mutants as opposed to its more ubiquitously expressed (and germline excluded) paralogs *ucr-2.1/2.2* affect cell nonautonomous UPR^{MT}. Beyond its role in the electron transport chain, there could also be a specific activity related to *ucr-2.3* in generating a signal either required for germline mitochondrial integrity or germline-to-intestine UPR^{MT} signaling. One possibility we considered is the predicted role of *ucr-2.3* as a protease, as its protein sequence is predicted to belong to the M16 metallopeptidase family, which includes mitochondrial processing peptidases. Indeed, the mammalian ortholog of *ucr-2.3*, UQCRC2, and its complex III core subunit partner UQCRC1 are homologous to the α-MPP and β-MPP (mitochondrial processing peptidase) subunits. Indeed, the mammalian ortholog of *ucr-2.3*, UQCRC2, is also predicted to have MPP-like (mitochondrial peptide processing) protease activity in combination with UQCRC1 to cleave off the N-terminal MTS of UQCRFS1(the Rieske Fe-S protein) in the final steps of complex III assembly (Deng et al., 2001, 1998; Fernandez-Vizarra and Zeviani, 2018). Whether *C. elegans* UCR-2.3 could also have an MPP-like role in complex III assembly in the germline or have an additional peptidase

role to generate peptide-like signals in the context of mitochondrial stress are interesting hypotheses that should be further explored.

Our results provide additional context for understanding the communication between germline and somatic tissues in regulating organismal health, specifically regarding mitochondrial quality. While sometimes regarded as two separate entities, the soma and the germline must engage in constant communication with each other to ensure overall organismal health (Conine and Rando, 2022). This can come in the form of small RNAs, nutrients, and other growth or stress cues that allow the germline to adapt to sources of environmental or somatic stress and, conversely, allow the somatic tissues to respond to changes in germline integrity. Several examples of soma-to-germline communication pathways have been described in *C. elegans* (Calculli et al., 2021; Curran et al., 2009; Shi and Murphy, 2023). One primary example of this is that signals from the reproductive system upon ablation of germline precursor stem cells activate the DAF-16/FOXO transcription factor in the intestine, which then increases lifespan and stress resistance (Arantes-Oliveira et al., 2002; Hsin and Kenyon, 1999). This was found to operate through activity of the cytochrome P450 enzyme DAF-9 which synthesized a steroid hormone recognized by the nuclear hormone receptor DAF-12 and ankyrin-repeat protein KRI-1 to regulate DAF-16 nuclear localization and activation in the intestine (Antebi et al., 2000; Berman and Kenyon, 2006; Gerisch et al., 2001). Our study adds to this work by connecting DAF-9 activity to reproductive signals and UPR^{MT} activation and lipid levels in the intestine. It will be interesting in future studies to understand how loss of UCR-2.3 influences DAF-9 activity and how DAF-9 steroid synthesis intersects with UPR^{MT} and lipid metabolism pathways.

While several reports of germline deficient animals have increased stress resistance for the cytosolic HSR or lifespan phenotypes (Hsin and Kenyon, 1999; Labbadia and Morimoto, 2015),

we find the opposite for mitochondrial stress responses; specifically, that germline deficiency shuts down UPR^{MT} signaling. We believe this specificity in germ cell regulation of mitochondrial stress signaling may result from a special requirement of mitochondrial quality in the germline. Because of the high abundance of mitochondria in germ cells and their important role in germ cell maturation (Van Blerkom, 2011; N. Zhang et al., 2021), the integrity of the germline and its consequential communication with other tissues may have a heavy reliance on mitochondrial quality. Indeed, oocytes in *C. elegans*, *Xenopus*, and humans employ specialized mechanisms to maintain mitochondrial quality and ensure integrity of the reproductive tissues (Colnaghi et al., 2021; Cota and Murphy, 2021; Rodríguez-Nuevo et al., 2022). Our results also highlight the importance of mitochondrial quality in germ tissue and suggest the possibility that integrity of germline may also regulate stress signaling pathways between the germline and somatic tissues. It will be important to understand whether these germline-somatic mitochondrial stress signaling pathways also are relevant for other forms of somatic stress besides proteotoxic PolyQ40 aggregation, such as obesity or infection, and what implications stresses occurring in the somatic tissues may have on germline mitochondrial quality, fertility or reproductive tissue health, and lipid metabolism.

Finally, it is intriguing to consider our results in the context of the "Disposable Soma Theory" which contends that there is an energetic trade-off between somatic maintenance and reproductive health. By this theory, animals lacking a germline should be able to invest more energetic resources to health maintenance in the somatic tissues, leading to increased longevity and stress resistance. Our observations provide another layer of complexity to this theory by contending that there may be an energetic triage occurring in response to loss of germline tissue. While loss of germline tissue or *ucr-2.3* may lead to the up-regulation of certain stress responses,

it leads to an intestinal UPR^{MT} shutdown. This may operate through signaling mechanisms specific to mitochondrial health or mitochondrial substrate requirements for metabolism no longer necessary in an infertile organism. Thus, this intestinal UPR^{MT} shut off could be an adaptive mechanism to conserve organismal resources but have additional consequences on fat metabolism or steroid hormone signaling in somatic tissues. Whether infertility or compromised reproductive tissues health may have similar consequences in mitochondrial or metabolic states in humans is of great future interest.

Figure legends

Figure 1: Mutagenesis screen reveals the requirement of *ucr-2.3* in neuron-to-intestine UPR^{MT} signaling

a. Schematic of cell nonautonomous UPR^{MT} signaling model in *C. elegans*. Through an inter-tissue signaling mechanism, neuron-specific mitochondrial stress activates the UPR^{MT} in the intestine of *C. elegans*. Neuronal mitochondrial stress can be induced by neuron-specific expression of a mutant, aggregation-prone PolyQ40 protein (*rgef-1p::Q40::YFP*) or neuron-specific knockdown mitochondrial genes like complex IV subunit *cco-1*. UPR^{MT} activation can be detected by use of a transcriptional reporter *hsp-6p::GFP*. See text for more details.
b. Fluorescence imaging and quantification of *rgef-1p::Q40::YFP; hsp-6p::GFP* animals with and without loss of function mutation *ucr-2.3(uth252)*. The Q40::YFP signal in *C. elegans* neurons is denoted with an orange arrowhead. The UPR^{MT} transcriptional reporter signal (GFP expression driven by the *hsp-6* promoter) is denoted with the red brackets. Significance determined by Welch's unpaired t-test, ****$p<0.0001$; $n > 3$.

c. Fluorescence imaging and quantification of *sid-1(qt9); rab-3p::cco-1* hairpin*; hsp-6p::GFP* animals with and without loss of function mutation *ucr-2.3(uth252)*. Significance determined by Welch's unpaired t-test, ****p<0.0001; n > 3.

d. Fluorescence imaging and quantification of *hsp-6p::GFP* animals with and without loss of function mutation *ucr-2.3(uth252)* fed *cco-1* RNAi . Significance determined by Welch's unpaired t-test, p = 0.6372; n > 3.

Supplementary Figure 1: Additional genetic evidence supporting loss of function mutations in *ucr-2.3* suppress cell nonautonomous UPR^{MT} signaling in *C. elegans*

a. Fluorescence imaging comparison of the wildtype UPR^{MT} cell nonautonomous reporter strain *rgef-1p::Q40::YFP;hsp-6p::GFP* to the EMS mutant obtained in the suppressor screen *uth16*. n> 3.

b. Fluorescence imaging comparison of a loss of function mutation in *ucr-2.3* generated by CRISPR/Cas9 genome editing to a non-edited, wildtype strain of *rgef-1p::Q40::YFP;hsp-6p::GFP*. n > 3.

c. *(i)* Fluorescence imaging comparison of a large deletion mutation in *ucr-2.3* compared to a wildtype strain of *rgef-1p::Q40::YFP;hsp-6p::GFP*. Quantification shown in (*ii*). Significance determined by Welch's unpaired t-test, p = 0.0010; n > 3.

d. qPCR comparison of *ucr-2.3* expression levels in wildtype and *ucr-2.3(uth252)* mutant animals in the *rgef-1p::Q40::YFP; hsp-6p::GFP* genetic background. Transcript levels normalized by *rpl-32*. Significance determined by Welch's unpaired t-test, **p=0.0016.

e. Fluorescence imaging showing autonomous UPR^{MT} activation comparing wildtype and *ucr-2.3(uth252)* animals fed *cco-1* RNAi in the *rgef-1p::Q40::YFP;hsp-6p::GFP* genetic background. n > 3.

f. Schematic describing genetic changes in all shown mutant alleles of *ucr-2.3*.

g. Fluorescence comparison of intestinal UPR^{MT} signal in wildtype and *ucr-2.3(uth252)* mutant animals over adult aging (Day 1 – 4 of adulthood). n > 3.

Figure 2: UCR-2.3 is a mitochondrial protein in *C. elegans* with a novel role in cell nonautonomous mitochondrial stress signaling

a. *(i)* Schematic of sub-cellular fractionation of a *C. elegans* strain with a HA-tag inserted at the C-terminus of the *ucr-2.3* genomic locus using CRISPR/Cas9 genomic editing. Cytosolic and mitochondrial fractions were run on a western blot probed with an HA antibody (to detect UCR-2.3 protein), a NDUFS3 antibody (to detect an established mitochondrial ETC protein), and an α-tubulin antibody (to detect an established cytosolic protein).

b. *(i)* Live-cell imaging showing sub-cellular localization of *C. elegans* UCR-2.3 in human RPE1 hTert cells transduced with *C. elegans* UCR2.3 tagged with mNeonGreen (UCR-2.3-mNG) and OMP25 tagged with BFP (OMP25-tagBFP2). Scale bar is 5 μm. *(ii)* Close up of two example regions shown in *(i)*. Scale bar is 1 μm. Data shown is representative of at least two independent imaging experiments with 5-10 images collected per cell line.

c. Measurement of mitochondrial respiration (oxygen consumption rate) between wildtype and the *ucr-2.3(uth252)* mutant in the *rgef-1p::Q40::YFP; hsp-6p::GFP* genetic background. Significance determined by Welch's unpaired t-test, ** p = 0.0079; n > 4.

d. Fluorescence imaging comparison of intestinal UPR^{MT} between wildtype and a *ucr-2.3* mutant with the predicted mitochondrial targeting sequence (MTS) deleted *ucr-2.3(ΔMTS)*, all in the *rgef-1p::Q40::YFP; hsp-6p::GFP* genetic background. Significance determined by Welch's unpaired t-test, * p = 0.0103; n = 3.

Supplementary Figure 2: *ucr-2.3* loss of function does not suppress UPR^{ER} or cytosolic HSR cell nonautonomous signaling

a. Fluorescence imaging comparison of the cell nonautonomous UPR^{ER} reporter strain (*rgef-1p::xbp-1s OE; hsp-4p::GFP*) with and without the *ucr-2.3(uth252)* loss of function mutation. Significance determined by Welch's unpaired t-test, ** p = 0.0055; n = 3.
b. Fluorescence imaging comparison of the cell nonautonomous HSR reporter strain (*rab-3p::hsf-1 OE; hsp-16p::GFP)* with and without the *ucr-2.3(uth252)* loss of function mutation. Significance determined by Welch's unpaired t-test, **** p < 0.0001; n = 2.
c. qPCR comparison of *ucr-2.3* expression levels in wildtype and *ucr-2.3(ΔMTS)* mutant animals in the *rgef-1p::Q40::YFP; hsp-6p::GFP* genetic background. Transcript levels normalized by *rpl-32*. Significance determined by Welch's unpaired t-test, p = 0.1603.

Figure 3: *ucr-2.3* is part of the UCR-2 family of gene paralogs that differ in their tissue expression and role in cell nonautonomous UPR^{MT} signaling

a. Human UQCRC2 is homologous to a family of UCR-2 genes in *C. elegans* including *ucr-2.1*, *ucr-2.2*, and *ucr-2.3*.
b. *(i)* Fluorescence imaging of comparing the loss of function mutations in the UCR-2 family on cell nonautonomous UPR^{MT} signaling. All mutations showed are nonsense-mediated

decay mutations generated via CRISPR/Cas9 editing. Quantification (*ii*). Significance determined by Welch's unpaired t-test. *p < 0.05, ****p < 0.0001; n = 3.

c. Fluorescence imaging comparison of tissue expression patterns across the UCR-2 family genes using an endogenous transcriptional reporter for each gene: *ucr-2.1* (*i*), *ucr-2.2* (*ii*), and *ucr-2.3* (*iii*). To generate each transcriptional reporter, a mCherry::GSG linker::F2A sequence was inserted between the gene promoter and coding region at the genomic locus using CRISPR/Cas9 editing.

d. Close up head images of the endogenous transcriptional reporter as described in (C).

e. Close up head imaging of *ucr-2.3* endogenous transcriptional reporter crossed to a *rgef-1p::GFP* reporter strain, expressing GFP in neurons.

Supplementary Figure 3: *ucr-2.1* and *ucr-2.2* are functionally redundant and display similar tissue expression patterns but differ from *ucr-2.3*

a. Measurement of mitochondrial respiration (oxygen consumption rate) upon *ucr-2.1* and *ucr-2.2* single and double RNAi knockdown in the *hsp-6p::GFP* genetic background. Significance determined by Welch's unpaired t-test. ****p<0.0001, non-significant p values > 0.4; n = 3.

b. Fluorescence imaging comparison of UPR^{MT} activation from *ucr-2.1* and *ucr-2.2* single and double RNAi knockdowns in the *hsp-6p::GFP* UPR^{MT} reporter strain. n = 3.

c. Fluorescence imaging comparison of UPR^{MT} activation from *ucr-2.1* and *ucr-2.2* single and double RNAi knockdowns in the *ucr-2.3(uth252); rgef-1p::Q40::YFP; hsp-6p::GFP* genetic background. n = 3.

d. qPCR measurement of relative transcript levels of the *ucr-2* family genes between the *ucr-2.3(uth252)* loss of function mutant and wildtype in the *rgef-1p::Q40::YFP; hsp-6p::GFP* genetic background.

e. qPCR measurement of relative transcript levels of the *ucr-2* family genes between the *ucr-2.1(uth267)* mutant *(i)* and *ucr-2.2(uth263)* mutant *(ii)* and wildtype with RNAi single and double knockdown of *ucr-2.1* and *ucr-2.2 (iii)* in the *rgef-1p::Q40::YFP; hsp-6p::GFP* genetic background.

f. Comparison of tissue-expression profiles for the UCR-2 family genes. Plots were generated using the Worm tissue expression prediction web interface (Kaletsky et al., 2018) (http:// https://worm.princeton.edu/).

Figure 4: Germline-specific expression of *ucr-2.3* can rescue cell nonautonomous UPR^{MT} signaling suppressed by the *ucr-2.3* loss of function mutation

a. Schematic of single-copy (mosSCI) tissue-specific rescue experiment. *ucr-2.3(ok3073)* mutant was crossed to strains containing an integrated, single-copy (mosSCI) of wildtype *ucr-2.3* driven by either a neuron-specific (*rgef-1p*) or germline-specific (*pie-1p*) promoter, all in the *rgef-1p::Q40::YFP; hsp-6p::GFP* genetic background.

b. Fluorescence imaging comparison of tissue-specific mosSCI rescue experiment in the *rgef-1p::Q40::YFP; hsp-6p::GFP* genetic background for the *ucr-2.3(ok3073)* mutation with tissue-specific rescue of wild-type *ucr-2.3* expressed in either in neurons (+ *rgef-1p*) or the germline (+ *pie-1p*) *(i)*. Significance determined by Welch's unpaired t-test, ****$p < 0.0001$. All non-significant p values > 0.3924. Quantification *(ii)*. n = 3.

c. Measurement of total brood size among wildtype, *ucr-2.3(ok3073)* loss of function mutant, and tissue-specific rescue with wild-type *ucr-2.3* expressed either in neurons (*rgef-1p::ucr-2.3*) or the germline (*pie-1p::ucr-2.3*), all in the *rgef-1p::Q40::YFP; hsp-6p::GFP* genetic background. Significance determined by Welch's unpaired t-test, **p=0.0011. All non-significant p values > 0.1507. n = 3.

d. Measurement of mitochondrial respiration (oxygen consumption rate) for wildtype and the *ucr-2.3(uth252)* mutant with and without an intact germline, all in the *rgef-1p::Q40::YFP; hsp-6p::GFP* genetic background. The germline was genetically ablated via the *glp-4(bn2)* temperature-sensitive mutant strain and conducting the entire experiment at the restrictive temperature 25°C. All strains were fed control HT115 RNAi bacteria, except for the *glp-4(bn2)* mutant animals fed *cco-1* RNAi. Significance determined by Welch's unpaired t-test, **p=0.0019, ****p < 0.0001, non-significant p = 0.1051. n = 3.

e. Fluorescence widefield imaging of *pie-1p::tomm-20::mKate2* germline mitochondrial reporter strain with and without the *ucr-2.3(uth252)* mutation *(i)*. Scale bar = 25 μm. Distal germ cells (green arrowhead) and oocytes (blue arrowhead) are shown in zoomed in images *(ii)*. Scale bar = 10 μm. Images shown are representative of at least 5-10 animals imaged per strain in at least three independent experiments each.

Supplementary Figure 4: Additional genetic evidence supporting a germline-specific role for *ucr-2.3* in mediating cell nonautonomous UPR^{MT}

a. *(i)* Fluorescence imaging comparison of intestinal UPR^{MT} signal between *ucr-2.3* excised only in neurons using FLP/FRT recombination (*ucr-2.3(FRT); rgef-1p::*FLP) compared to *ucr-2.3* with the FRT sites alone *ucr-2.3(FRT)*, all in the *rgef-1p::Q40::YFP; hsp-6p::GFP*

genetic background. Wildtype and *ucr-2.3(uth252)* loss of function mutant displayed for comparison. *(ii)* Quantification. Significance determined by Welch's unpaired t-test, **p=0.0052, non-significant p values > 0.4. n = 3. *(iii)* DNA gel displaying excised *ucr-2.3* upon FLP/FRT recombination by PCR genotyping the *ucr-2.3* genetic locus in each strain listed.

Figure 5: *ucr-2.3* operates downstream of established neuronal factors in mediating cell nonautonomous UPR^{MT}

a. Schematic of known neuronal molecular players that mediate cell nonautonomous UPR^{MT} signaling between neurons and the intestine in *C. elegans.*
b. Fluorescence imaging comparison and quantification of intestinal mtUPR signal in the *rgef-1p::jmjd-1.2; hsp-6p::GFP* strain with and without the *ucr-2.3(uth252)* mutation. Significance determined by Welch's unpaired t-test, ***p=0.0004; n = 3.
c. Fluorescence imaging comparison and quantification of intestinal mtUPR signal in the *rgef-1p::egl-20; hsp-6p::GFP* strain with and without the *ucr-2.3(uth252)* mutation Significance determined by Welch's unpaired t-test, **p=0.0052; n = 3.
d. Fluorescence imaging comparison of intestinal UPR^{MT} signal for exogenous addition of serotonin (5-HT) to *rgef-1p::Q40::YFP; hsp-6p::GFP* animals in the wildtype or *ucr-2.3(uth252)* loss of function mutant. Quantification shows fold change in intestinal UPR^{MT} fluorescence upon serotonin (5-HT) addition. Significance determined by Welch's unpaired t-test, * p = 0.0296, non-significant p value = 0.3129. n = 4.

Figure 6: The germline, and especially germline mitochondria, is required for UPR^{MT} non-autonomous signaling.

a. Comparison of fluorescence imaging and quantification of intestinal UPR^{MT} signal in *(i) glp-4(bn2)* or *(ii) glp-1(e2141)* temperature sensitive mutants, all in the *rgef-1p::Q40::YFP; hsp-6p::GFP* background, or *(iii) glp-4(bn2)* in the *sid-1(qt9); rab-3p::cco-1 hairpin; hsp-6p::GFP* background. Experiment conducted at the restrictive temperature 25 °C to deplete the germline. Significance determined by Welch's unpaired t-test, ****, *** $p<0.0001$; n = 3.

b. Comparison of fluorescence imaging and respective quantification of intestinal UPR^{MT} signal upon FUDR treatment for germline mitochondria depletion in the *(i) rgef-1p::Q40::YFP; hsp-6p::GFP* background or the *(ii) glp-4(bn2)* in the *sid-1(qt9); rab-3p::cco-1 hairpin; hsp-6p::GFP* background. Significance determined by Welch's unpaired t-test, **$p = 0.0034$, **** $p<0.0001$; n = 3.

Supplementary Figure 5: Additional evidence supporting a specific role for the germline in mediating UPR^{MT} signaling

a. *(i)* Fluorescence imaging comparison of intestinal UPR^{MT} signal for RNAi knockdown of UPR^{MT} factors *atfs-1*, *egl-20*, and *jmjd-1.2* in a germline-specific RNAi strain (Zou et al., 2019) crossed to the cell nonautonomous UPRMT reporter: *sun-1p::rde-1; rde-1(mkc36); rgef-1p::Q40::YFP; hsp-6p::GFP*. *(ii)* RNAi knockdown of the same UPR^{MT} factors in the standard cell nonautonomous UPR^{MT} reporter *rgef-1p::Q40::YFP; hsp-6p::GFP*. n = 3.

b. Fluorescence widefield imaging of *pie-1p::tomm-20::mKate2* germline mitochondrial reporter strain with and without FUDR treatment.

c. Fluorescence imaging comparison and quantification of the cell nonautonomous UPR^{ER} *(i)* and cytosolic HSR *(ii)* reporter strains upon germline depletion by FUDR treatment. Significance determined by Welch's unpaired t-test, *(i)* $p = 0.5250$. *(ii)* **** $p < 0.0001$. n = 3.

d. Fluorescence imaging comparison and quantification of the cell nonautonomous UPR^{ER} and HSR reporter strains upon genetic germline depletion by the *glp-4(bn2)* temperature sensitive mutation at the restrictive temperature 25 °C. Images shown are representative of three independent experiments. Quantification displays average fluorescence values for each strain from three independent experiments. Significance determined by Welch's paired t-test across the three independent experiments, *(i)* $p = 0.7477$; *(ii)* $p = 0.6100$.

Figure 7: The germline communicates via a steroid hormone signaling to regulate intestinal UPR^{MT} activation.

a. Comparison of lipid levels and quantification of Nile Red fluorescence between wildtype and the *ucr-2.3(uth252)* mutant. Significance determined by Welch's unpaired t-test, ****$p < 0.0001$; n = 3.

b. Comparison of fluorescence imaging and quantification of intestinal UPR^{MT} signal for the *ucr-2.3(uth252)* mutant or *ucr-2.3(uth252); daf-9(rh50)* double mutant in the *rgef-1p::Q40::YFP; hsp-6p::GFP* genetic background. Significance determined by Welch's unpaired t-test, ***$p = 0.0004$; n = 3.

c. Oil Red O staining and quantification of lipid levels in the *ucr-2.3(uth252)* mutant or *ucr-2.3(uth252); daf-9(rh50)* double mutant in the *rgef-1p::Q40::YFP; hsp-6p::GFP* genetic background. Significance determined by Welch's unpaired t-test, * $p = 0.0185$.

d. Proposed model for how germline mitochondria mediate neuron-to-intestine UPR^{MT} stress signaling. *(i)* Parallel Signaling pathway (Dashed lines): Neurons can communicate to the intestine, or the germline. Simultaneously, the germline acts as a master switch to control "ON"/"OFF" ability for the UPR^{MT} to be activated in the intestine, regardless of presence of other signals. *(ii)* Direct Signaling pathway (Solid lines): Neurons directly communicate to the germline, which processes signals perhaps through mitochondrial activity, then sends a signal to the intestine to regulate UPR^{MT} activation.

Supplementary Figure 6: Increased intestinal fat levels in *ucr-2.3* loss of function mutant

a. Oil Red O staining and quantification of lipid levels in wildtype or *ucr-2.3(uth252)* mutant animals. Significance determined by Welch's unpaired t-test, ** $p = 0.0185$; $n = 2$.

Methods

C. elegans strain generation and maintenance

C. elegans animals were fed standard OP50 bacteria and grown on standard NGM containing media. For all RNAi knockdown experiments, *C. elegans* animals were fed HT115 bacteria expressing dsRNA targeted to the gene of interest on NGM media containing IPTG and appropriate antibiotics for selection of the dsRNA-containing plasmid. All strains were either generated by this study, generated by SUNY Biotech, or ordered from the Caenorhabditis Genetics Center (CGC). The only exception is the SJZ106 strain (*foxSi27[pie-1p::tomm20::mKate2::HA::tbb-2 3'UTR]*), which was a kind gift from Dr. Steve Zuryn (The University of Queensland). CRISPR-edited strains were either ordered from SUNY Biotech or generated by this study following standard *C. elegans* CRISPR/Cas9 genome editing protocols

(Arribere et al., 2014) and the Alt-R CRISPR-Cas9 system (IDT). Briefly, Cas9 protein (UC Berkeley QB3 MacroLab) was combined with Alt-R CRISPR tracrRNA, a crRNA mixture (targeted to our gene of interest and *dpy-10*), and ssDNA repair template mixture (again, targeted to our gene of interest and *dpy-10*) as a ribonucleoprotein complex and injected into the gonad of L4 stage *C. elegans* hermaphrodites. This allowed us to select "jackpot" broods containing many F1 animals with "roller" or "dumpy" phenotypes to improve efficiency in selection of broods with edited genomes. mosSCI integration of strains were generated following standard procedures (Frøkjær-Jensen et al., 2008). Briefly, constructs of interest were cloned into the pCFJ356 mosSCI plasmid backbone. A DNA mixture of the mosSCI plasmid of interest, the pCFJ601 plasmid (containing the mosSCI transposase), and mCherry expressing plasmids (to eliminate non-integrated, array animals) was injected into the gonad of young, "uncoordinated" EG6703 animals. Resulting progeny were screened for broods that yielded only "mover" animals with no mCherry-expressing arrays.

Animal synchronization and maintenance

Unless stated, all experiments were performed with synchronization using a standard hypochlorite treatment protocol. Briefly, animals were washed off NGM plates with a M9 solution and bleached with 1.8% sodium hypochlorite solution until all animal carcasses were disintegrated. Resulting eggs were washed five times with M9 solution using centrifugation and eggs were plated on respective plates for the experiments. All experiments were conducted at 20 °C except for germline ablation experiments with temperature sensitive mutants, which were done at the restrictive temperature of 25 °C as indicated in figure legends.

Mutagenesis screen

rgef-1p::Q40::YFP; hsp-6p::GFP animals at the L4 stage were incubated with Ethyl-methyl sulfonate (EMS, Sigma). Five plates of 250 F1 progeny each were selected to screen 2500 genomes. F2 progeny were screened for suppression of *hsp-6p::GFP* signal in the intestine. Identified suppressors were singled onto fresh plates and further screened for homozygous, recessive mutations. Selected suppressor mutants were backcrossed to the parental strain carrying the reporter and polyQ transgenes at least one time.

Mutation mapping

We followed a SNP-based whole genome sequencing method to identify putative causative mutations in the suppressor mutants (Doitsidou et al., 2010). Briefly, we outcrossed suppressor mutant strains with males from a Hawaiian CB4866 strain containing the *rgef-1p::Q40::YFP* and *hsp-6p::GFP* transgenes. F2 progeny containing the suppression phenotype were selected and allowed to self-fertilize for two generations. Then, genomic DNA was extracted from these suppressor lines using the DNeasy kit (Qiagen) and sent to the Beijing Genomics Institute for WGS on their Illumina HiSeq platform using single 90 nucleotide reads. Genomic data was analyzed using MAQgene as previously described (Bigelow et al., 2009; Doitsidou et al., 2010).

Fluorescence stereoscope imaging and quantification

Animals were synchronized by hypochlorite treatment and hatched on either control or respective HT115 RNAi bacteria. Animals were grown to Day 2 at 20 °C unless otherwise indicated, like for the restrictive temperature experiments. For imaging experiments in the *rab-3p::hsf-1 OE; hsp-16.2p::GFP* background, animals were heatshocked for imaging as had been previously published

(Gildea et al., 2022). Briefly, animals were hatched and allowed to develop at either 20 °C or 25 °C (if a temperature sensitive mutant). On the day of the experiment, animals were then heatshocked at 34 °C for 2 hr, then let recover at their original temperature they developed at for 2 hr, then imaged. For imaging, D2 animals were anesthesized with 0.1 M sodium azide and lined up on an NGM plate without a bacterial lawn. Animals were imaged using M250FA stereoscope (Leica) under respective fluorescence. Animals were imaged at 250ms exposure under GFP excitation fluorescence unless otherwise indicated. Quantification of intestinal GFP signal was performed using ImageJ/FIJI by tracing the intestinal regions. Statistical analyses were performed with GraphPad PRISM as described in the figure legends.

Quantitative RT-PCR

Synchronized animals were collected on Day 2 of adulthood and gravity washed in M9 buffer to isolate adults and remove larvae. Animals were collected in three independent biological replicates for one experiment. Washed animals were then frozen in TRIzol (Invitrogen) and freeze thawed using liquid nitrogen. RNA was harvested from animals using a TRIzol-based extraction method and RNA was purified using a RNeasy Mini Kit (Qiagen). cDNA was synthesized using the QuantiTect Reverse Transcription Kit (Qiagen) using equivalent amounts of RNA per sample. qPCR was performed using a standard curve protocol using SYBR Select Master Mix (Life Technologies). Statistical analyses were performed with GraphPad PRISM as described in the figure legends. Primers used are:

Gene	Forward primer	Reverse primer
rpl-32	AGGGAATTGATAACCGTGTCCGCA	TGTAGGACTGCATGAGGAGCATGT
ucr-2.1	TTGAACTAAACGGAGCCAC	TAAGTCCTTGCTTGTTGGC
ucr-2.2	CGAGGATGTGCTGCCAACTA	CGAAGTGCTGCTCTGCAAAT
ucr-2.3	GGAGTGTGGTGTCGTACCAG	GCGATAGTCTCCACCCCTGA

Sub-cellular fractionation and western blotting

Sub-cellular fractionation and mitochondrial enrichment of *C. elegans* lysates was performed as previously described (Xin et al., 2022). Briefly, synchronized animals were mechanically homogenized with a Dura-Grind Stainless Steel Dounce Trissue Grinder (Wheaton) in mitochondrial extraction buffer (5 mM Tris-HCl / 7.4, 210 mM mannitol, 70 mM sucrose, and 0.1 mM EDTA) with protease inhibitor. Lysates were subject to differential centrifugation. Protein concentration was measured using a Rapid Gold BCA kit (Pierce) before being loaded onto Tris-Glycine 4-12% gels (Invitrogen). Gels were transferred using NuPAGE transfer buffer (Invitrogen) onto nitrocellulose membranes (Biorad) and blocked with LI-COR Blocking Buffer (LI-COR) with Tween. Membranes were probed with antibodies targeted to HA (Abcam, ab9110), NDUFS3 (Abcam, ab14711), and α Tubulin (Sigma, T9026).

Cell culture, virus generation and transduction

Human hTERT-RPE-1 PAC knockout cells (gifted by Andrew Holland (Lambrus et al., 2016)) were grown in DMEM:F-12 (Gibco) supplemented with 10% FBS (VWR Scientific), 1% Glutamax (Gibco), 1% NEAA (Gibco), and 1% Penicillin/Streptomycin (Gibco). HEK-293T cells were grown in DMEM (GIBCO) containing 10% FBS (VWR Scientific), 1% Glutamax (Gibco), 1% NEAA (Gibco), and 1% Penicillin/Streptomycin (Gibco). Cells were maintained at 37° C with 5% CO_2 at atmospheric O_2. Cultures were passaged enzymatically every 3-4 days using 0.25% Trypsin (Gibco) diluted 1:3 in 1X PBS (Gibco). Trypsin was inactivated by cell media.

Cloning of plasmids for cell culture

C. elegans (human codon-optimized) UCR-2.3-mNeonGreen and OMP25-tagBFP2 were synthesized as geneblocks (IDT), PCR amplified with Q5 polymerase (New England Biolabs) and incubated with restriction enzyme-digested CD510-B1 plasmid (SystemBio) and assembled with Gibson Assembly Master Mix (New England Biolabs).

Generation and transduction of UCR-2.3 lentivirus

Lentiviral plasmids encoding pCMV-OMP25-tagBFP2-EF1a-NEO and pUbC-UCR-2.3-mNeonGreen-EF1a-Puro were transfected into HEK-293T cells with lentiviral packaging plasmids with Lipofectamine 3000 (Invitrogen) according to standard lentiviral production protocols. Viral supernatant was filtered through a 0.45 µm filter before transduction. RPE-1 cells were transduced with lentivirus at an MOI of 0.3-0.5 (usually between 50-100 µL of virus/well) and 10 µg/mL Polybrene (Sigma-Aldrich). After 48 hours, RPE-1 cell media was replaced and grown in the presence of 1 µg/mL Puromycin (Gibco) or 100 µg/mL Geneticin (Gibco) for about 7 days and until all non-transduced control cells died.

Live cell microscopy of human cells

RPE-1 cells were seeded at 1.25 x 10^5 cells/dish onto Fibronectin-coated plates, 35-mm glass-bottom dishes with #1.5 cover glass (Cellvis) 24 hours prior to imaging. Prior to live cell imaging, cell medium was replaced with pre-warmed FluoroBrite DMEM (Gibco) supplemented with 10% FBS, 1% Glutamax, 1% NEAA, 1% Penicillin/Streptomycin, 1 µM SYTO Deep Red Fluorescent Nuclei Acid Stain (Invitrogen), and 1 µM Probenecid (Invitrogen). Imaging of live cells was performed with a Zeiss Airyscan microscope LSM900 equipped with heated stage and environmental chamber maintained at 37° C and 5% CO_2. Images were acquired using the

ZenBlue3.1 software followed by deconvolution and Airyscan processing, and further processed using ImageJ/FIJI.

Mitochondrial oxygen consumption assays

All mitochondrial oxygen consumption rate assays (OCR) were performed using a Seahorse XFe96 Analyzer (Agilent) at 20 °C following a previously published protocol . Briefly, the sensor cartridge was calibrated the day before at room temperature, and appropriate drugs (NaN_3, FCCP) were loaded into the injection ports. Day 2 adult animals were gravity washed with M9 buffer, then loaded 10-20 animals per well into the cell culture plate. After respirometry run was completed, the number of animals were counted per well to normalize the data. Statistical analyses were performed with GraphPad PRISM as described in the figure legends.

Fluorescence widefield microscopy of *C. elegans*

Slides for imaging were prepared by making a fresh flattened 5% agarose pad. Animals were immobilized in 12 µl of 0.1% NaN_3, then sealed beneath a 22x22mm coverglass. 6-10 animals were imaged per condition per experiment. Imaging was done using a Leica DM6 Thunder Imager and processed using LAS X software automated Thunder small volume computational clearing.

Brood size assay

For each strain tested, five L4 animals were singled onto OP50 bacterial plates and kept at 20 °C to lay. Animals were moved each day to new OP50 plates until Day 5. Progeny laid by each singled animal were counted at the L4 or Day 1 life stage. Statistical analyses were performed with GraphPad PRISM as described in the figure legends.

Exogenous serotonin addition

Exogenous serotonin addition was performed following a published procedure (Berendzen et al., 2016). Serotonin hydrochloride (Sigma) was solubilized in MilliQ water and plated onto NGM agar plates already containing control HT115 RNAi bacteria. Solubilized serotonin concentrations were calculated so that the final serotonin concentration as stated considers the total agar volume of the plate (approximately 9.9 ml). Seeded serotonin plates were allowed to dry overnight in the dark and plated with eggs harvested from a hypochlorite treatment for the experiment.

5-Fluoro-2'deoxyuridine (FUDR) treatment

Eggs were harvested from hypochlorite treatment of animals and plated on control HT115 bacterial plates. 100 μL of 10 mg/mL FUDR was seeded onto the control HT115 bacterial lawn and let dry overnight at room temperature. At the L4 developmental stage, animals were moved onto the FUDR-treatment plates and let grown to Day 2 of adulthood for their respective experiment.

Oil Red O and Nile Red staining

Lipid staining using Oil Red O or Nile Red was conducted following previously published protocol (Escorcia et al., 2018). Briefly, synchronized animals were grown to Day 2 on respective HT115 RNAi media. Animals were washed in PBS-T, fixed in 40% isopropanol, then incubated with Oil Red O or Nile Red stain for 2 hours at room temperature shielded from light. Excess dye was washed off and animals were imaged via fluorescence stereoscope imaging for Nile Red using a M250FA stereoscope (Leica) or brightfield/colorimetric imaging for Oil Red O using a Revolve microscope (Echo). Quantification of signal was performed in ImageJ by tracing intestinal regions

for fluorescent Nile Red images or Oil Red O colorimetric images. For quantification, Oil Red O images were transformed into the HIS color space using the Color Transformer 2 plugin and quantified in the (S) channel. Statistical analyses were performed with GraphPad PRISM as described in the figure legends.

Acknowledgements: We thank all members of the Dillin lab, Dr. Jeremy Chang, Dr. Veerle Rottiers, and Dr. Malene Hansen for their feedback on the project.

References

Ahier, A., Dai, C.-Y., Tweedie, A., Bezawork-Geleta, A., Kirmes, I., Zuryn, S., 2018. Affinity purification of cell-specific mitochondria from whole animals resolves patterns of genetic mosaicism. Nat. Cell Biol. 20, 352–360. https://doi.org/10.1038/s41556-017-0023-x

Antebi, A., Yeh, W.-H., Tait, D., Hedgecock, E.M., Riddle, D.L., 2000. *daf-12* encodes a nuclear receptor that regulates the dauer diapause and developmental age in *C. elegans*. Genes Dev. 14, 1512–1527. https://doi.org/10.1101/gad.14.12.1512

Aprison, E.Z., Dzitoyeva, S., Ruvinsky, I., 2023. Serotonergic signaling plays a deeply conserved role in improving oocyte quality. Dev. Biol. 499, 24–30. https://doi.org/10.1016/j.ydbio.2023.04.008

Arantes-Oliveira, N., Apfeld, J., Dillin, A., Kenyon, C., 2002. Regulation of Life-Span by Germ-Line Stem Cells in *Caenorhabditis elegans*. Science 295, 502–505. https://doi.org/10.1126/science.1065768

Arribere, J.A., Bell, R.T., Fu, B.X.H., Artiles, K.L., Hartman, P.S., Fire, A.Z., 2014. Efficient Marker-Free Recovery of Custom Genetic Modifications with CRISPR/Cas9 in *Caenorhabditis elegans*. Genetics 198, 837–846. https://doi.org/10.1534/genetics.114.169730

Beanan, M.J., Strome, S., 1992. Characterization of a germ-line proliferation mutation in *C. elegans*. Development 116, 755–766. https://doi.org/10.1242/dev.116.3.755

Berendzen, K.M., Durieux, J., Shao, L.-W., Tian, Y., Kim, H., Wolff, S., Liu, Y., Dillin, A., 2016. Neuroendocrine Coordination of Mitochondrial Stress Signaling and Proteostasis. Cell 166, 1553-1563.e10. https://doi.org/10.1016/j.cell.2016.08.042

Berman, J.R., Kenyon, C., 2006. Germ-Cell Loss Extends C. elegans Life Span through Regulation of DAF-16 by kri-1 and Lipophilic-Hormone Signaling. Cell 124, 1055–1068. https://doi.org/10.1016/j.cell.2006.01.039

Bieri, G., Schroer, A.B., Villeda, S.A., 2023. Blood-to-brain communication in aging and rejuvenation. Nat. Neurosci. https://doi.org/10.1038/s41593-022-01238-8

Bigelow, H., Doitsidou, M., Sarin, S., Hobert, O., 2009. MAQGene: software to facilitate C. elegans mutant genome sequence analysis. Nat. Methods 6, 549–549. https://doi.org/10.1038/nmeth.f.260

Birch, J., Gil, J., 2020. Senescence and the SASP: many therapeutic avenues. Genes Dev. 34, 1565–1576. https://doi.org/10.1101/gad.343129.120

Calculli, G., Lee, H.J., Shen, K., Pham, U., Herholz, M., Trifunovic, A., Dillin, A., Vilchez, D., 2021. Systemic regulation of mitochondria by germline proteostasis prevents protein aggregation in the soma of *C. elegans*. Sci. Adv. 7, eabg3012. https://doi.org/10.1126/sciadv.abg3012

Cao, J., Packer, J.S., Ramani, V., Cusanovich, D.A., Huynh, C., Daza, R., Qiu, X., Lee, C., Furlan, S.N., Steemers, F.J., Adey, A., Waterston, R.H., Trapnell, C., Shendure, J., 2017. Comprehensive single-cell transcriptional profiling of a multicellular organism. Science 357, 661–667. https://doi.org/10.1126/science.aam8940

Castillo-Armengol, J., Fajas, L., Lopez-Mejia, I.C., 2019. Inter-organ communication: a gatekeeper for metabolic health. EMBO Rep. 20, e47903. https://doi.org/10.15252/embr.201947903

Chandel, N.S., 2014. Mitochondria as signaling organelles. BMC Biol. 12, 34. https://doi.org/10.1186/1741-7007-12-34

Colnaghi, M., Pomiankowski, A., Lane, N., 2021. The need for high-quality oocyte mitochondria at extreme ploidy dictates mammalian germline development. eLife 10, e69344. https://doi.org/10.7554/eLife.69344

Conine, C.C., Rando, O.J., 2022. Soma-to-germline RNA communication. Nat. Rev. Genet. 23, 73–88. https://doi.org/10.1038/s41576-021-00412-1

Cota, V., Murphy, C.T., 2021. Fission and PINK-1-mediated mitophagy are required for Insulin/IGF-1 signaling mutant reproductive longevity (preprint). Genetics. https://doi.org/10.1101/2021.08.16.456566

Curran, S.P., Wu, X., Riedel, C.G., Ruvkun, G., 2009. A soma-to-germline transformation in long-lived Caenorhabditis elegans mutants. Nature 459, 1079–1084. https://doi.org/10.1038/nature08106

Deng, K., Shenoy, S.K., Tso, S.-C., Yu, L., Yu, C.-A., 2001. Reconstitution of Mitochondrial Processing Peptidase from the Core Proteins (Subunits I and II) of Bovine Heart Mitochondrial

Cytochrome bc1 Complex. J. Biol. Chem. 276, 6499–6505. https://doi.org/10.1074/jbc.M007128200

Deng, K., Zhang, L., Kachurin, A.M., Yu, L., Xia, D., Kim, H., Deisenhofer, J., Yu, C.-A., 1998. Activation of a Matrix Processing Peptidase from the Crystalline Cytochrome bc1 Complex of Bovine Heart Mitochondria. J. Biol. Chem. 273, 20752–20757. https://doi.org/10.1074/jbc.273.33.20752

Doitsidou, M., Poole, R.J., Sarin, S., Bigelow, H., Hobert, O., 2010. C. elegans Mutant Identification with a One-Step Whole-Genome-Sequencing and SNP Mapping Strategy. PLoS ONE 5, e15435. https://doi.org/10.1371/journal.pone.0015435

Durieux, J., Wolff, S., Dillin, A., 2011. The Cell-Non-Autonomous Nature of Electron Transport Chain-Mediated Longevity. Cell 144, 79–91. https://doi.org/10.1016/j.cell.2010.12.016

Escorcia, W., Ruter, D.L., Nhan, J., Curran, S.P., 2018. Quantification of Lipid Abundance and Evaluation of Lipid Distribution in Caenorhabditis elegans by Nile Red and Oil Red O Staining. J. Vis. Exp. 57352. https://doi.org/10.3791/57352

Fernandez-Vizarra, E., Zeviani, M., 2018. Mitochondrial complex III Rieske Fe-S protein processing and assembly. Cell Cycle 17, 681–687. https://doi.org/10.1080/15384101.2017.1417707

Frøkjær-Jensen, C., Wayne Davis, M., Hopkins, C.E., Newman, B.J., Thummel, J.M., Olesen, S.-P., Grunnet, M., Jorgensen, E.M., 2008. Single-copy insertion of transgenes in Caenorhabditis elegans. Nat. Genet. 40, 1375–1383. https://doi.org/10.1038/ng.248

Fukasawa, Y., Tsuji, J., Fu, S.-C., Tomii, K., Horton, P., Imai, K., 2015. MitoFates: Improved Prediction of Mitochondrial Targeting Sequences and Their Cleavage Sites*. Mol. Cell. Proteomics 14, 1113–1126. https://doi.org/10.1074/mcp.M114.043083

Gerisch, B., Weitzel, C., Kober-Eisermann, C., Rottiers, V., Antebi, A., 2001. A Hormonal Signaling Pathway Influencing C. elegans Metabolism, Reproductive Development, and Life Span. Dev. Cell 1, 841–851. https://doi.org/10.1016/S1534-5807(01)00085-5

Gildea, H.K., Frankino, P.A., Tronnes, S.U., Pender, C.L., Durieux, J., Dishart, J.G., Choi, H.O., Hunter, T.D., Cheung, S.S., Frakes, A.E., Sukarto, E., Wickham, K., Dillin, A., 2022. Glia of *C. elegans* coordinate a protective organismal heat shock response independent of the neuronal thermosensory circuit. Sci. Adv. 8, eabq3970. https://doi.org/10.1126/sciadv.abq3970

Greer, E.L., Maures, T.J., Hauswirth, A.G., Green, E.M., Leeman, D.S., Maro, G.S., Han, S., Banko, M.R., Gozani, O., Brunet, A., 2010. Members of the H3K4 trimethylation complex regulate lifespan in a germline-dependent manner in C. elegans. Nature 466, 383–387. https://doi.org/10.1038/nature09195

Han, S., Schroeder, E.A., Silva-García, C.G., Hebestreit, K., Mair, W.B., Brunet, A., 2017. Mono-unsaturated fatty acids link H3K4me3 modifiers to C. elegans lifespan. Nature 544, 185–190. https://doi.org/10.1038/nature21686

Horowitz, A.M., Fan, X., Bieri, G., Smith, L.K., Sanchez-Diaz, C.I., Schroer, A.B., Gontier, G., Casaletto, K.B., Kramer, J.H., Williams, K.E., Villeda, S.A., 2020. Blood factors transfer beneficial effects of exercise on neurogenesis and cognition to the aged brain. Science 369, 167–173. https://doi.org/10.1126/science.aaw2622

Houtkooper, R.H., Mouchiroud, L., Ryu, D., Moullan, N., Katsyuba, E., Knott, G., Williams, R.W., Auwerx, J., 2013. Mitonuclear protein imbalance as a conserved longevity mechanism. Nature 497, 451–457. https://doi.org/10.1038/nature12188

Howe, K.L., Bolt, B.J., Cain, S., Chan, J., Chen, W.J., Davis, P., Done, J., Down, T., Gao, S., Grove, C., Harris, T.W., Kishore, R., Lee, R., Lomax, J., Li, Y., Muller, H.-M., Nakamura, C., Nuin, P., Paulini, M., Raciti, D., Schindelman, G., Stanley, E., Tuli, M.A., Van Auken, K., Wang, D., Wang, X., Williams, G., Wright, A., Yook, K., Berriman, M., Kersey, P., Schedl, T., Stein, L., Sternberg, P.W., 2016. WormBase 2016: expanding to enable helminth genomic research. Nucleic Acids Res. 44, D774–D780. https://doi.org/10.1093/nar/gkv1217

Hsin, H., Kenyon, C., 1999. Signals from the reproductive system regulate the lifespan of C. elegans. Nature 399, 362–366. https://doi.org/10.1038/20694

Iwata, S., Lee, J.W., Okada, K., Lee, J.K., Iwata, M., Rasmussen, B., Link, T.A., Ramaswamy, S., Jap, B.K., 1998. Complete Structure of the 11-Subunit Bovine Mitochondrial Cytochrome bc_1 Complex. Science 281, 64–71. https://doi.org/10.1126/science.281.5373.64

Jia, Q., Sieburth, D., 2021. Mitochondrial hydrogen peroxide positively regulates neuropeptide secretion during diet-induced activation of the oxidative stress response. Nat. Commun. 12, 2304. https://doi.org/10.1038/s41467-021-22561-x

Kaletsky, R., Yao, V., Williams, A., Runnels, A.M., Tadych, A., Zhou, S., Troyanskaya, O.G., Murphy, C.T., 2018. Transcriptome analysis of adult Caenorhabditis elegans cells reveals tissue-specific gene and isoform expression. PLOS Genet. 14, e1007559. https://doi.org/10.1371/journal.pgen.1007559

Kang, G.M., Min, S.H., Lee, C.H., Kim, J.Y., Lim, H.S., Choi, M.J., Jung, S.-B., Park, J.W., Kim, S., Park, C.B., Dugu, H., Choi, J.H., Jang, W.H., Park, S.E., Cho, Y.M., Kim, J.G., Kim, K.-G., Choi, C.S., Kim, Y.-B., Lee, C., Shong, M., Kim, M.-S., 2021. Mitohormesis in Hypothalamic POMC Neurons Mediates Regular Exercise-Induced High-Turnover Metabolism. Cell Metab. 33, 334-349.e6. https://doi.org/10.1016/j.cmet.2021.01.003

Katsimpardi, L., Litterman, N.K., Schein, P.A., Miller, C.M., Loffredo, F.S., Wojtkiewicz, G.R., Chen, J.W., Lee, R.T., Wagers, A.J., Rubin, L.L., 2014. Vascular and Neurogenic Rejuvenation of the Aging Mouse Brain by Young Systemic Factors. Science 344, 630–634. https://doi.org/10.1126/science.1251141

Kim, H.-E., Grant, A.R., Simic, M.S., Kohnz, R.A., Nomura, D.K., Durieux, J., Riera, C.E., Sanchez, M., Kapernick, E., Wolff, S., Dillin, A., 2016. Lipid Biosynthesis Coordinates a Mitochondrial-to-Cytosolic Stress Response. Cell 166, 1539-1552.e16. https://doi.org/10.1016/j.cell.2016.08.027

Labbadia, J., Morimoto, R.I., 2015. Repression of the Heat Shock Response Is a Programmed Event at the Onset of Reproduction. Mol. Cell 59, 639–650. https://doi.org/10.1016/j.molcel.2015.06.027

Lambrus, B.G., Daggubati, V., Uetake, Y., Scott, P.M., Clutario, K.M., Sluder, G., Holland, A.J., 2016. A USP28–53BP1–p53–p21 signaling axis arrests growth after centrosome loss or prolonged mitosis. J. Cell Biol. 214, 143–153. https://doi.org/10.1083/jcb.201604054

Macías-León, J., Askjaer, P., 2018. Efficient FLP-mediated germ-line recombination in C. elegans. Micropublication.

Mello, C.C., Draper, B.W., Prless, J.R., 1994. The maternal genes apx-1 and glp-1 and establishment of dorsal-ventral polarity in the early C. elegans embryo. Cell 77, 95–106. https://doi.org/10.1016/0092-8674(94)90238-0

Merkwirth, C., Jovaisaite, V., Durieux, J., Matilainen, O., Jordan, S.D., Quiros, P.M., Steffen, K.K., Williams, E.G., Mouchiroud, L., Tronnes, S.U., Murillo, V., Wolff, S.C., Shaw, R.J., Auwerx, J., Dillin, A., 2016. Two Conserved Histone Demethylases Regulate Mitochondrial Stress-Induced Longevity. Cell 165, 1209–1223. https://doi.org/10.1016/j.cell.2016.04.012

Miller, W.L., 2013. Steroid hormone synthesis in mitochondria. Mol. Cell. Endocrinol. 379, 62–73. https://doi.org/10.1016/j.mce.2013.04.014

Moehle, E.A., Shen, K., Dillin, A., 2019. Mitochondrial proteostasis in the context of cellular and organismal health and aging. J. Biol. Chem. 294, 5396–5407. https://doi.org/10.1074/jbc.TM117.000893

Mottis, A., Herzig, S., Auwerx, J., 2019. Mitocellular communication: Shaping health and disease. Science 366, 827–832. https://doi.org/10.1126/science.aax3768

Muñoz-Jiménez, C., Ayuso, C., Dobrzynska, A., Torres-Mendéz, A., Ruiz, P. de la C., Askjaer, P., 2017. An Efficient FLP-Based Toolkit for Spatiotemporal Control of Gene Expression in *Caenorhabditis elegans*. Genetics 206, 1763–1778. https://doi.org/10.1534/genetics.117.201012

Nargund, A.M., Pellegrino, M.W., Fiorese, C.J., Baker, B.M., Haynes, C.M., 2012. Mitochondrial Import Efficiency of ATFS-1 Regulates Mitochondrial UPR Activation. Science 337, 587–590. https://doi.org/10.1126/science.1223560

Nomura, H., Athauda, S.B.P., Wada, H., Maruyama, Y., Takahashi, K., Inoue, H., 2006. Identification and Reverse Genetic Analysis of Mitochondrial Processing Peptidase and the Core Protein of the Cytochrome bc1 Complex of Caenorhabditis elegans, a Model Parasitic Nematode. J. Biochem. (Tokyo) 139, 967–979. https://doi.org/10.1093/jb/mvj114

Owusu-Ansah, E., Song, W., Perrimon, N., 2013. Muscle Mitohormesis Promotes Longevity via Systemic Repression of Insulin Signaling. Cell 155, 699–712. https://doi.org/10.1016/j.cell.2013.09.021

Ozek, C., Krolewski, R.C., Buchanan, S.M., Rubin, L.L., 2018. Growth Differentiation Factor 11 treatment leads to neuronal and vascular improvements in the hippocampus of aged mice. Sci. Rep. 8, 17293. https://doi.org/10.1038/s41598-018-35716-6

Rao, S., Schieber, A.M.P., O'Connor, C.P., Leblanc, M., Michel, D., Ayres, J.S., 2017. Pathogen-Mediated Inhibition of Anorexia Promotes Host Survival and Transmission. Cell 168, 503-516.e12. https://doi.org/10.1016/j.cell.2017.01.006

Rodríguez-Nuevo, A., Torres-Sanchez, A., Duran, J.M., De Guirior, C., Martínez-Zamora, M.A., Böke, E., 2022. Oocytes maintain ROS-free mitochondrial metabolism by suppressing complex I. Nature 607, 756–761. https://doi.org/10.1038/s41586-022-04979-5

Shao, L.-W., Niu, R., Liu, Y., 2016. Neuropeptide signals cell non-autonomous mitochondrial unfolded protein response. Cell Res. 26, 1182–1196. https://doi.org/10.1038/cr.2016.118

Shen, K., Pender, C.L., Bar-Ziv, R., Zhang, H., Wickham, K., Willey, E., Durieux, J., Ahmad, Q., Dillin, A., 2022. Mitochondria as Cellular and Organismal Signaling Hubs. Annu. Rev. Cell Dev. Biol. 38, annurev-cellbio-120420-015303. https://doi.org/10.1146/annurev-cellbio-120420-015303

Shi, C., Murphy, C.T., 2023. piRNAs regulate a Hedgehog germline-to-soma pro-aging signal. Nat. Aging 3, 47–63. https://doi.org/10.1038/s43587-022-00329-2

Shpilka, T., Haynes, C.M., 2018. The mitochondrial UPR: mechanisms, physiological functions and implications in ageing. Nat. Rev. Mol. Cell Biol. 19, 109–120. https://doi.org/10.1038/nrm.2017.110

Smith, H.J., Sharma, A., Mair, W.B., 2020. Metabolic Communication and Healthy Aging: Where Should We Focus Our Energy? Dev. Cell 54, 196–211. https://doi.org/10.1016/j.devcel.2020.06.011

TeKippe, M., Aballay, A., 2010. C. elegans Germline-Deficient Mutants Respond to Pathogen Infection Using Shared and Distinct Mechanisms. PLoS ONE 5, e11777. https://doi.org/10.1371/journal.pone.0011777

Tsang, W.Y., Lemire, B.D., 2002. Mitochondrial Genome Content Is Regulated during Nematode Development. Biochem. Biophys. Res. Commun. 291, 8–16. https://doi.org/10.1006/bbrc.2002.6394

Van Blerkom, J., 2011. Mitochondrial function in the human oocyte and embryo and their role in developmental competence. Mitochondrion 11, 797–813. https://doi.org/10.1016/j.mito.2010.09.012

Van Oosten-Hawle, P., 2023. Exploiting inter-tissue stress signaling mechanisms to preserve organismal proteostasis during aging. Front. Physiol. 14, 1228490. https://doi.org/10.3389/fphys.2023.1228490

Wang, M.C., O'Rourke, E.J., Ruvkun, G., 2008. Fat Metabolism Links Germline Stem Cells and Longevity in *C. elegans*. Science 322, 957–960. https://doi.org/10.1126/science.1162011

Xin, N., Durieux, J., Yang, C., Wolff, S., Kim, H.-E., Dillin, A., 2022. The UPR ^{mt} Preserves Mitochondrial Import to Extend Lifespan (preprint). Cell Biology. https://doi.org/10.1101/2020.07.01.182980

Zhang, N., Sun, A., Sun, S., Yang, R., Shi, Y., Wang, Q., Li, X., Ma, J., Yue, W., Xie, B., Qiao, J., Li, M., 2021. Mitochondrial proteome of mouse oocytes and cisplatin-induced shifts in protein profile. Acta Pharmacol. Sin. 42, 2144–2154. https://doi.org/10.1038/s41401-021-00687-4

Zhang, Q., Wang, Z., Zhang, W., Wen, Q., Li, X., Zhou, J., Wu, X., Guo, Y., Liu, Y., Wei, C., Qian, W., Tian, Y., 2021. The memory of neuronal mitochondrial stress is inherited transgenerationally via elevated mitochondrial DNA levels. Nat. Cell Biol. 23, 870–880. https://doi.org/10.1038/s41556-021-00724-8

Zhang, Q., Wu, X., Chen, P., Liu, L., Xin, N., Tian, Y., Dillin, A., 2018. The Mitochondrial Unfolded Protein Response Is Mediated Cell-Non-autonomously by Retromer-Dependent Wnt Signaling. Cell 174, 870-883.e17. https://doi.org/10.1016/j.cell.2018.06.029

Zou, L., Wu, D., Zang, X., Wang, Z., Wu, Z., Chen, D., 2019. Construction of a germline-specific RNAi tool in C. elegans. Sci. Rep. 9, 2354. https://doi.org/10.1038/s41598-019-38950-8

Figure 1

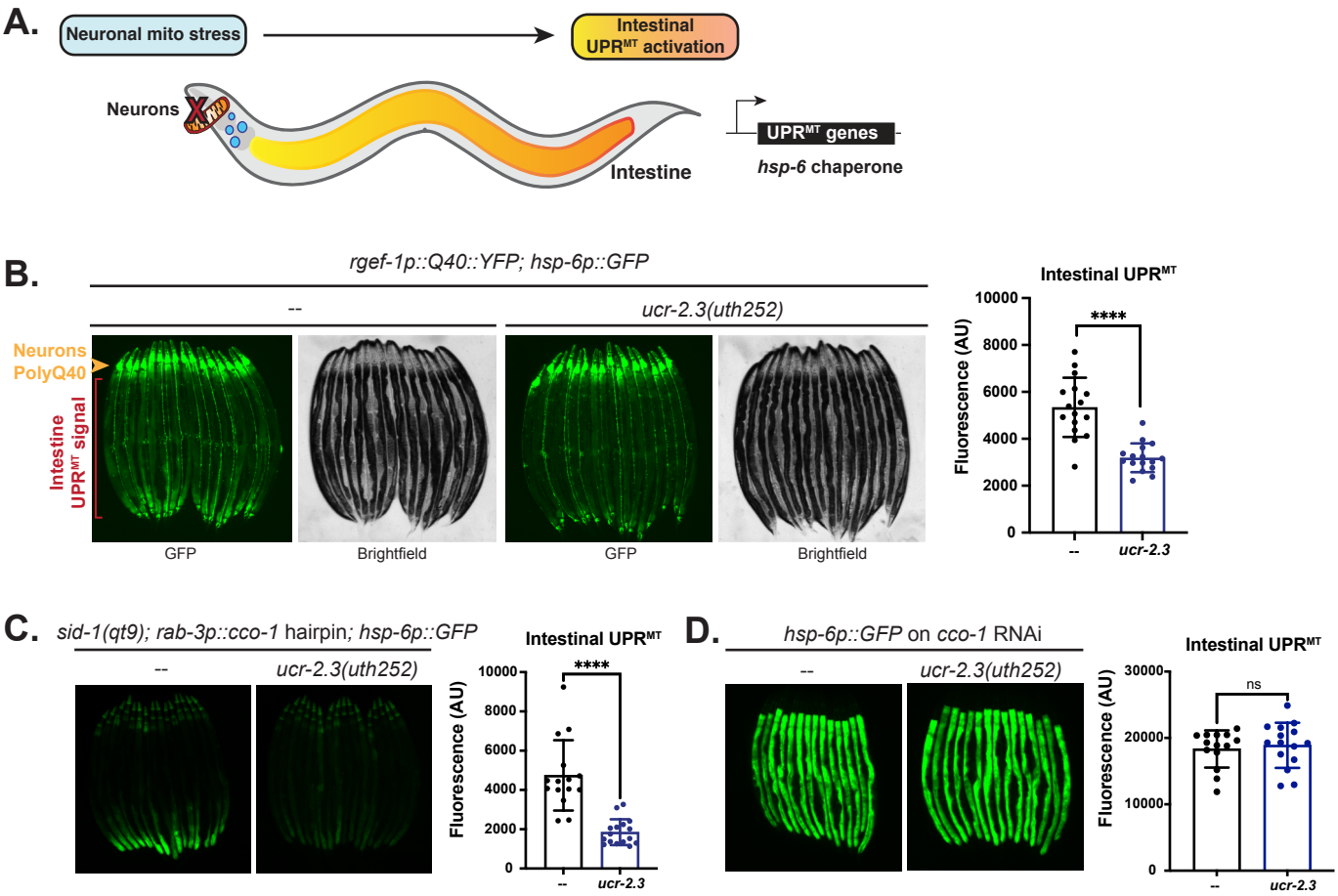
A.
Neuronal mito stress
Intestinal UPR^MT activation
Neurons
Intestine
UPR^MT genes
hsp-6 chaperone
B.
rgef-1p::Q40::YFP; hsp-6p::GFP
--
ucr-2.3(uth252)
Neurons PolyQ40
Intestine UPR^MT signal
GFP
Brightfield
GFP
Brightfield
Intestinal UPR^MT
Fluorescence (AU)
10000
8000
6000
4000
2000
0
****
--
ucr-2.3
C.
sid-1(qt9); rab-3p::cco-1 hairpin; hsp-6p::GFP
--
ucr-2.3(uth252)
Intestinal UPR^MT
Fluorescence (AU)
10000
8000
6000
4000
2000
0
****
--
ucr-2.3
D.
hsp-6p::GFP on cco-1 RNAi
--
ucr-2.3(uth252)
Intestinal UPR^MT
Fluorescence (AU)
30000
20000
10000
0
ns
--
ucr-2.3

Figure 2

A. *i.*

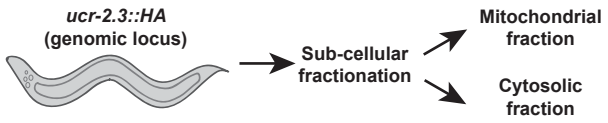

ii.

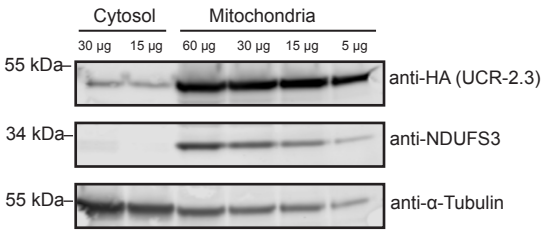

B. *i.*

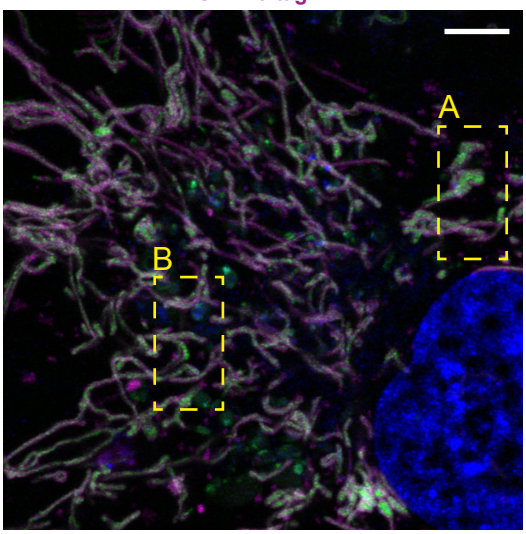

ii.

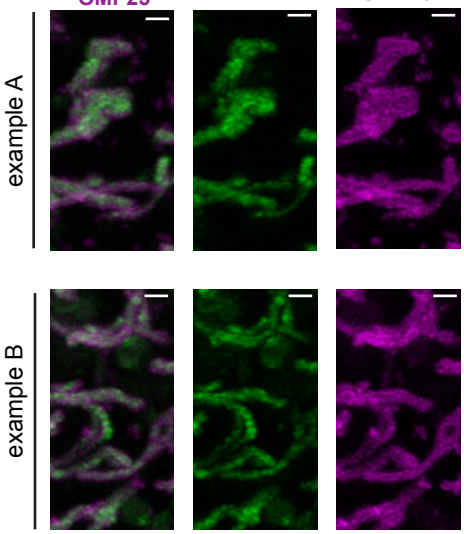

C.

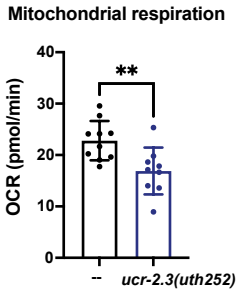

D.

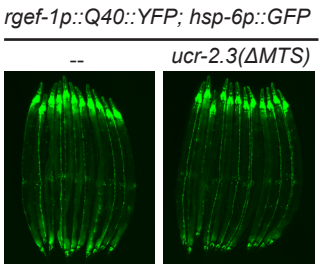

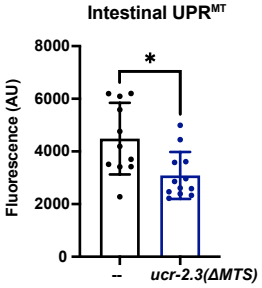

Figure 3

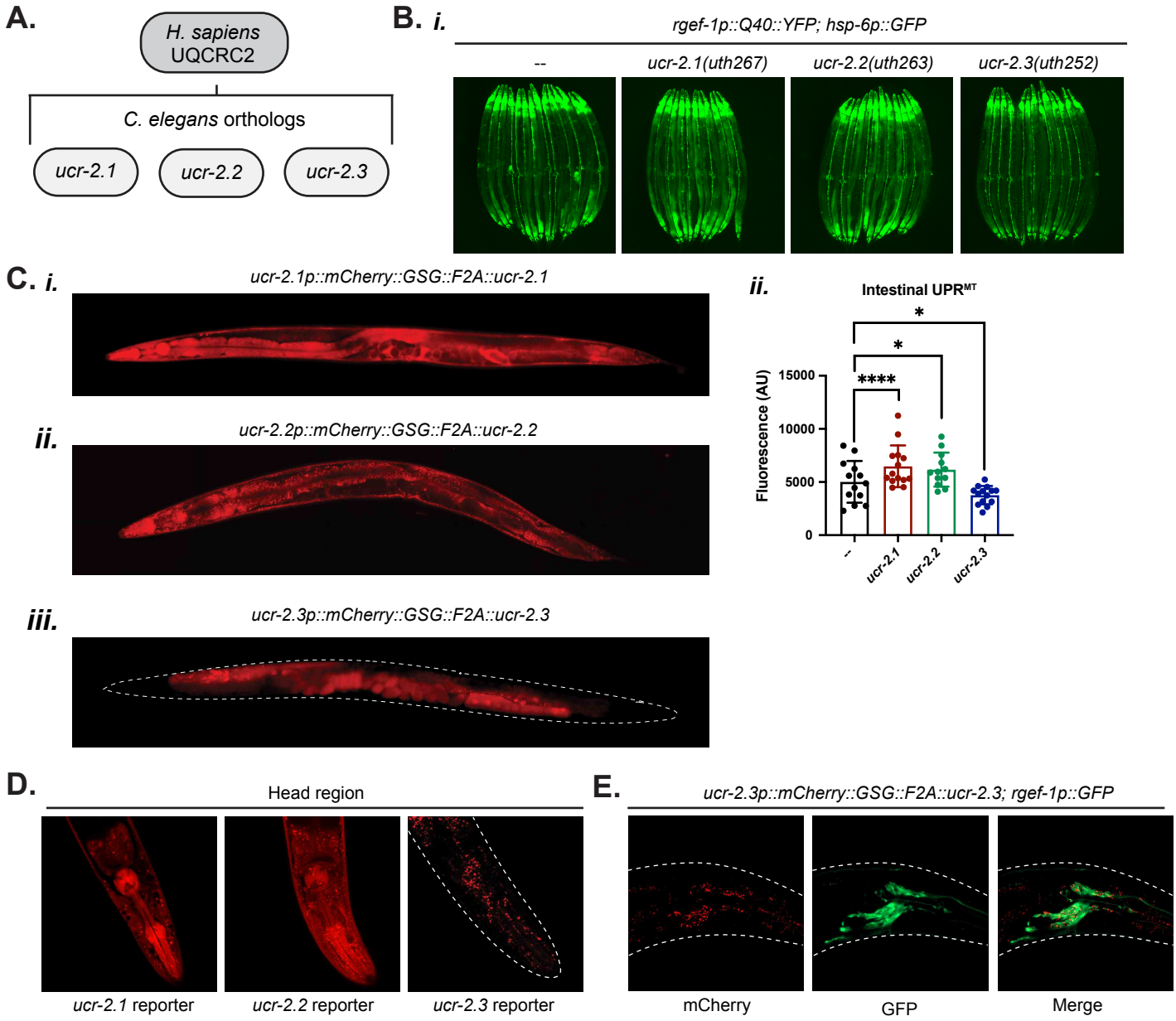
A.
H. sapiens UQCRC2
C. elegans orthologs
ucr-2.1
ucr-2.2
ucr-2.3
B. i.
rgef-1p::Q40::YFP; hsp-6p::GFP
--
ucr-2.1(uth267)
ucr-2.2(uth263)
ucr-2.3(uth252)
C. i.
ucr-2.1p::mCherry::GSG::F2A::ucr-2.1
ii.
ucr-2.2p::mCherry::GSG::F2A::ucr-2.2
iii.
ucr-2.3p::mCherry::GSG::F2A::ucr-2.3
ii.
Intestinal UPRMT
Fluorescence (AU)
15000
10000
5000
0
****
*
*
--
ucr-2.1
ucr-2.2
ucr-2.3
D.
Head region
ucr-2.1 reporter
ucr-2.2 reporter
ucr-2.3 reporter
E.
ucr-2.3p::mCherry::GSG::F2A::ucr-2.3; rgef-1p::GFP
mCherry
GFP
Merge

Figure 4

A. **Design of mosSCI tissue-specific rescue experiment:**

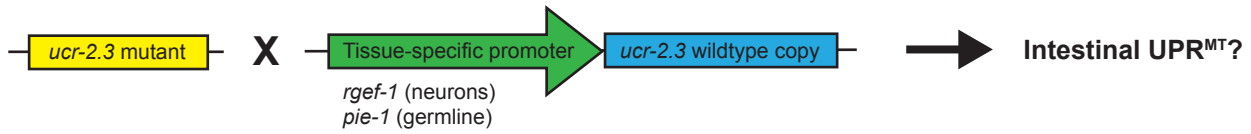

B. ***i.***

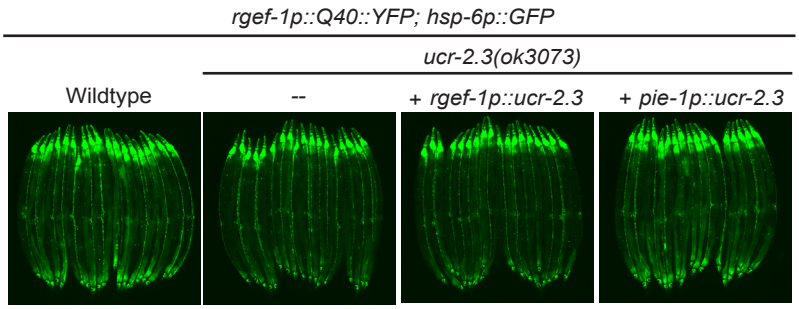

ii.

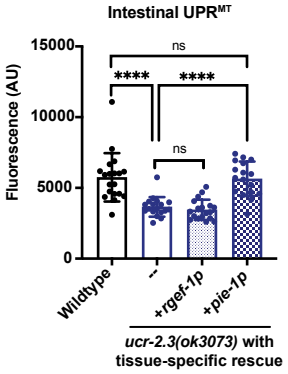

C.

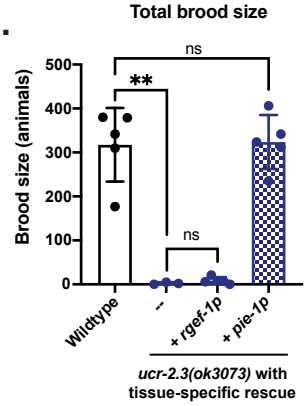

D.

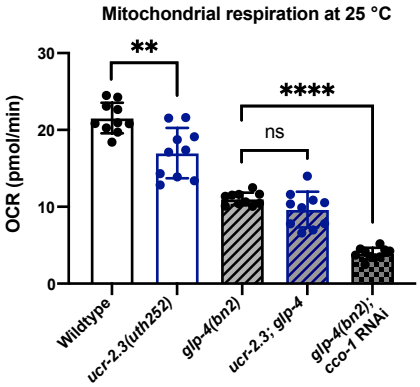

E. ***i.***

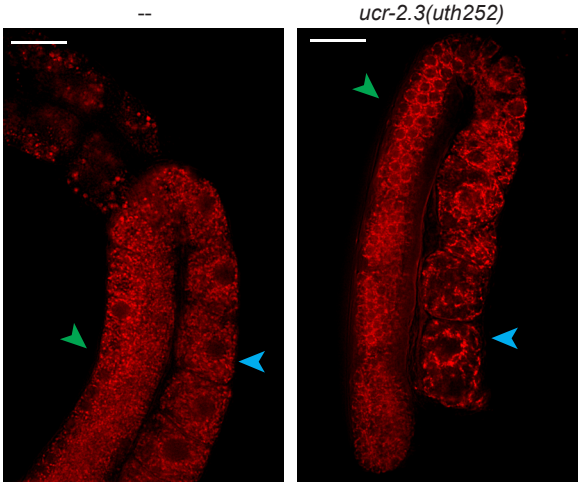

ii.

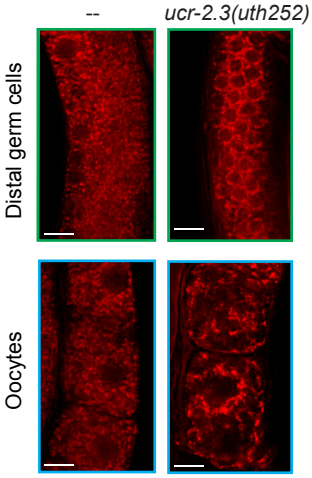

Figure 5

A.

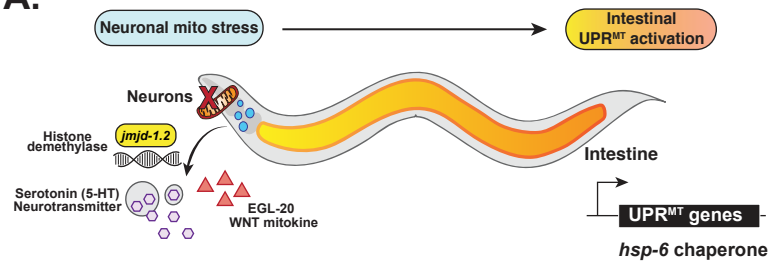

B.

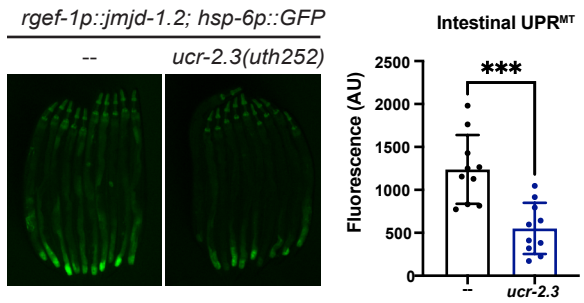

C.

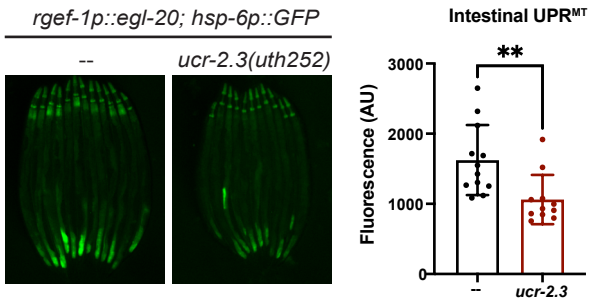

D.

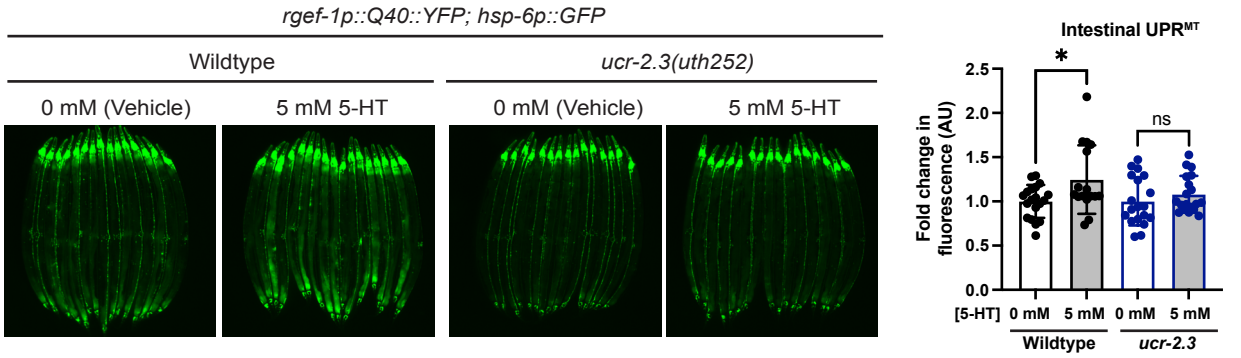

Figure 6

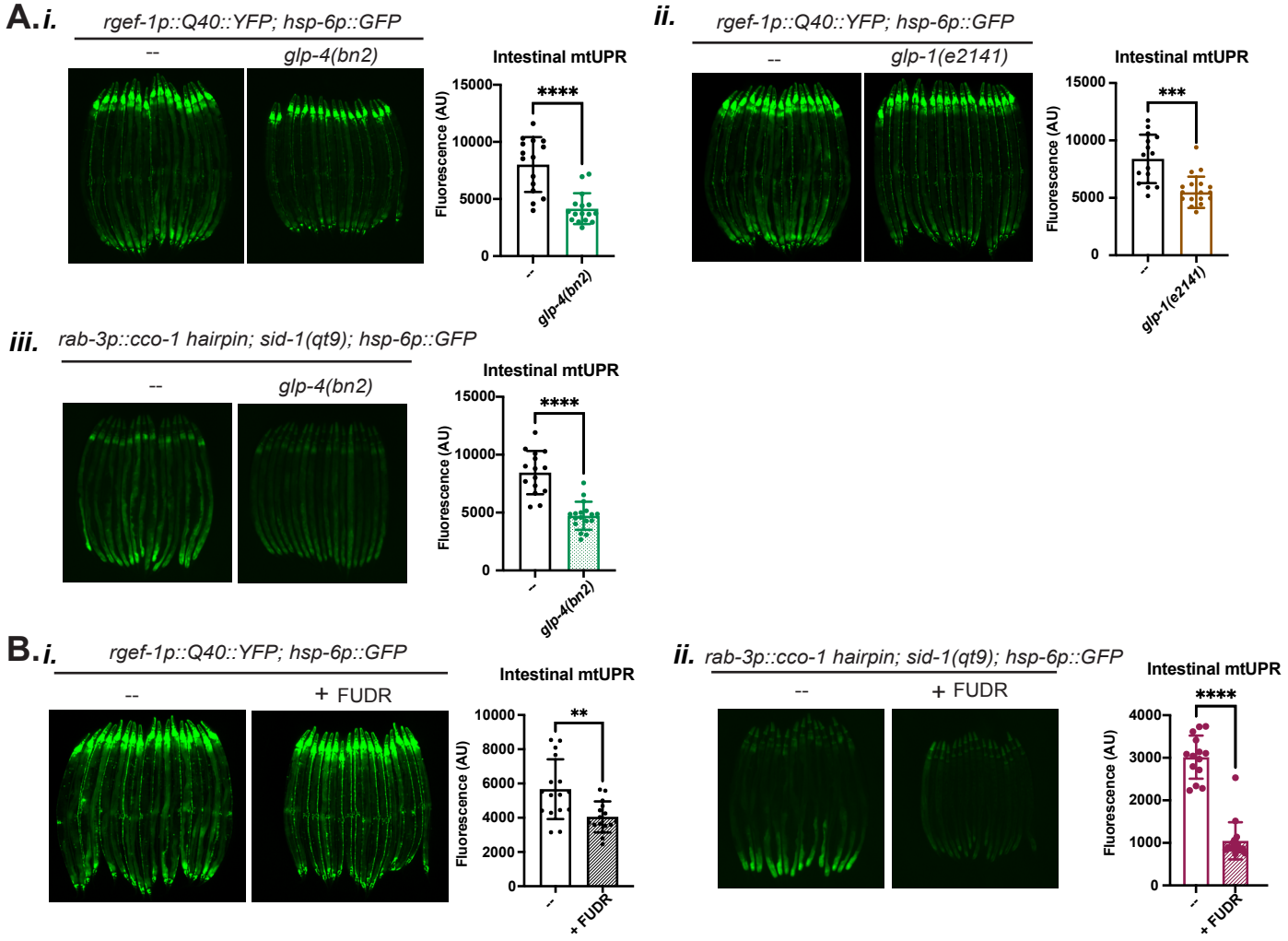
A. i.
rgef-1p::Q40::YFP; hsp-6p::GFP
--
glp-4(bn2)
Intestinal mtUPR
Fluorescence (AU)
15000
10000
5000
0
****
--
glp-4(bn2)
ii.
rgef-1p::Q40::YFP; hsp-6p::GFP
--
glp-1(e2141)
Intestinal mtUPR
Fluorescence (AU)
15000
10000
5000
0
***
--
glp-1(e2141)
iii.
rab-3p::cco-1 hairpin; sid-1(qt9); hsp-6p::GFP
--
glp-4(bn2)
Intestinal mtUPR
Fluorescence (AU)
15000
10000
5000
0
****
--
glp-4(bn2)
B. i.
rgef-1p::Q40::YFP; hsp-6p::GFP
--
+ FUDR
Intestinal mtUPR
Fluorescence (AU)
10000
8000
6000
4000
2000
0
**
--
+ FUDR
ii.
rab-3p::cco-1 hairpin; sid-1(qt9); hsp-6p::GFP
--
+ FUDR
Intestinal mtUPR
Fluorescence (AU)
4000
3000
2000
1000
0
****
--
+ FUDR

Figure 7

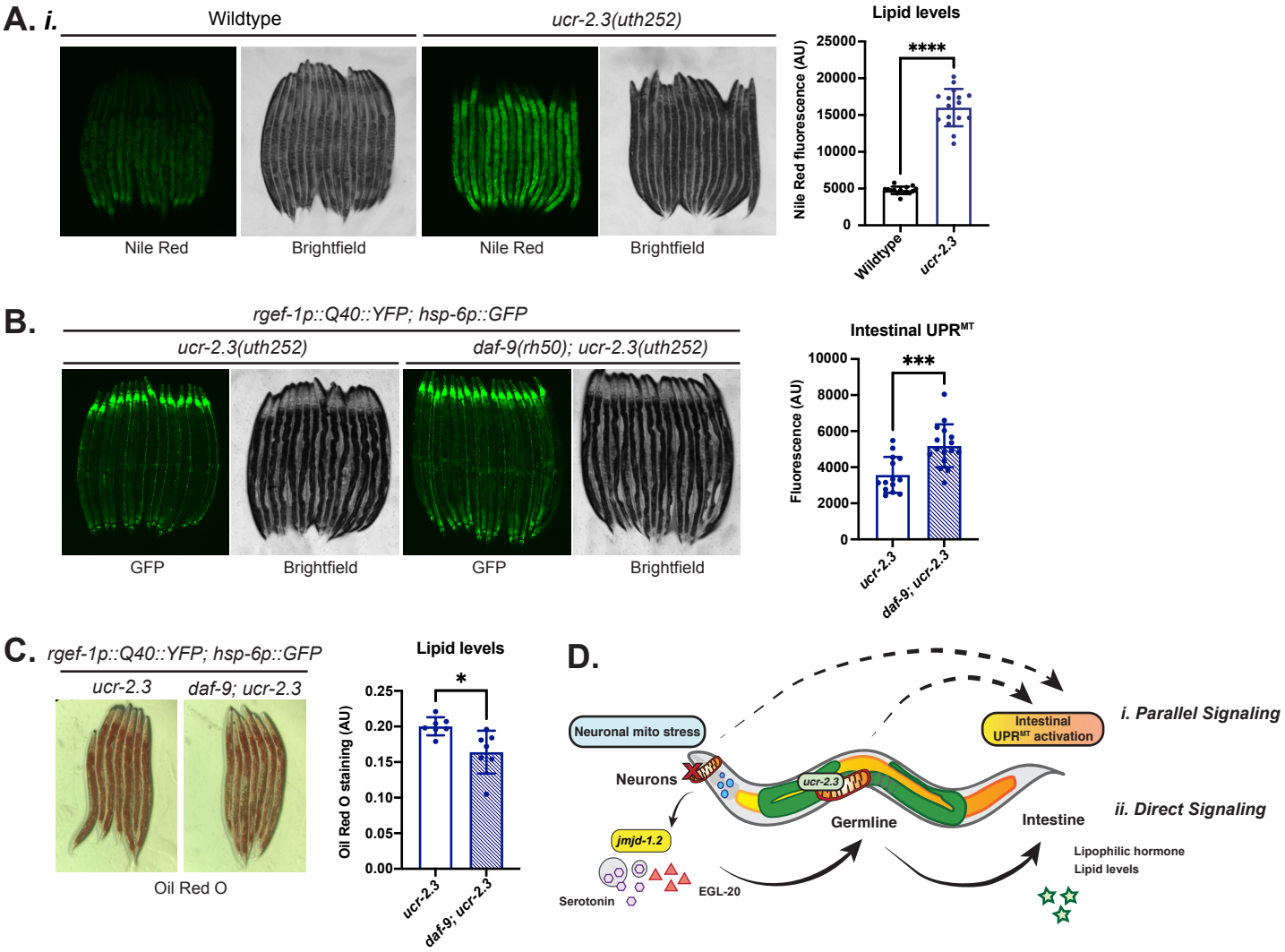
A. i.
Wildtype
ucr-2.3(uth252)
Nile Red
Brightfield
Nile Red
Brightfield
Lipid levels
Nile Red fluorescence (AU)
25000
20000
15000
10000
5000
0
****
Wildtype
ucr-2.3
B.
rgef-1p::Q40::YFP; hsp-6p::GFP
ucr-2.3(uth252)
daf-9(rh50); ucr-2.3(uth252)
GFP
Brightfield
GFP
Brightfield
Intestinal UPRMT
Fluorescence (AU)
10000
8000
6000
4000
2000
0
***
ucr-2.3
daf-9; ucr-2.3
C.
rgef-1p::Q40::YFP; hsp-6p::GFP
ucr-2.3
daf-9; ucr-2.3
Oil Red O
Lipid levels
Oil Red O staining (AU)
0.25
0.20
0.15
0.10
0.05
0.00
*
ucr-2.3
daf-9; ucr-2.3
D.
Neuronal mito stress
Intestinal UPRMT activation
i. Parallel Signaling
Neurons
ucr-2.3
Germline
Intestine
ii. Direct Signaling
jmjd-1.2
Serotonin
EGL-20
Lipophilic hormone
Lipid levels

Supplementary Figure 1

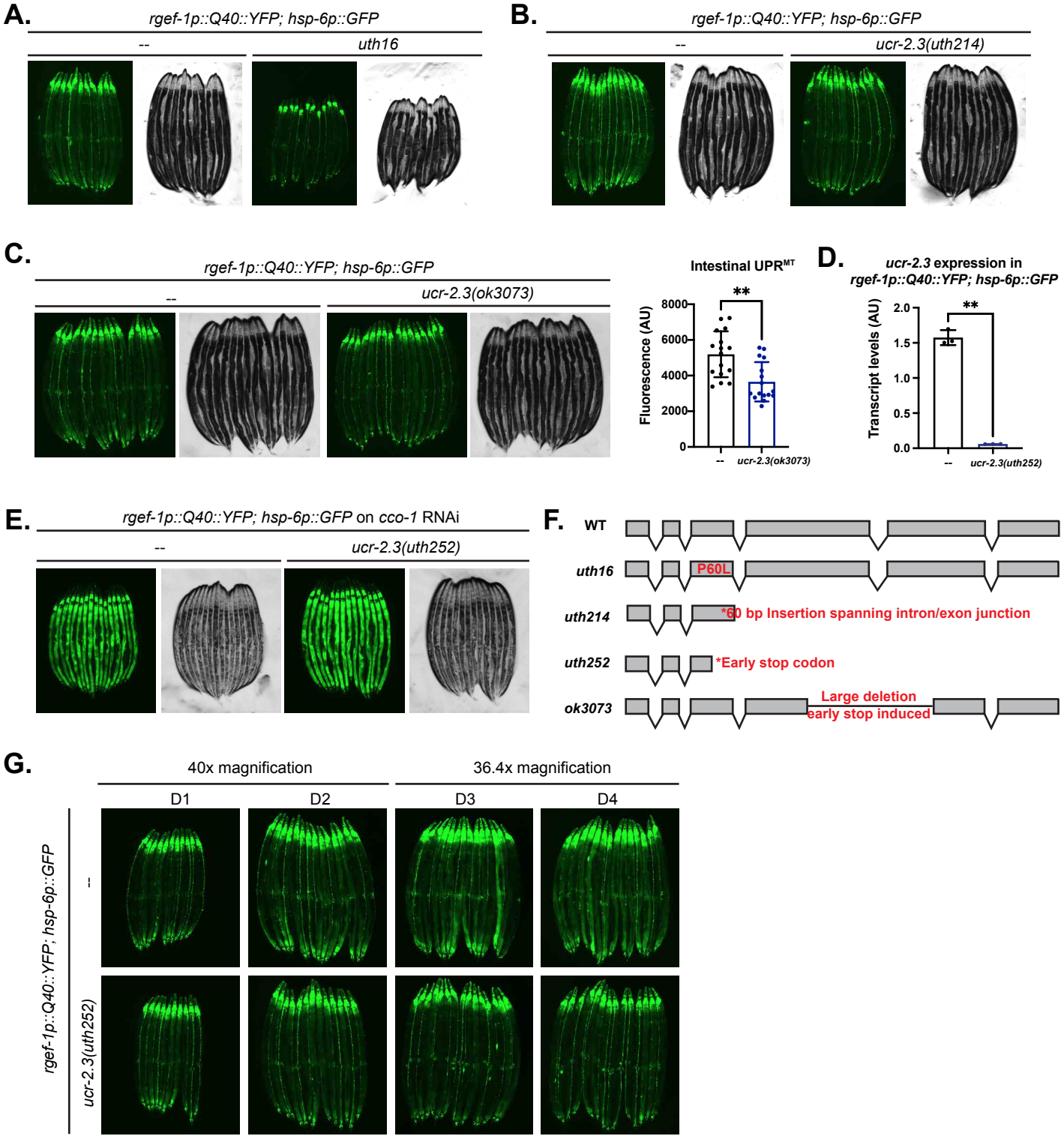

Supplementary Figure 2

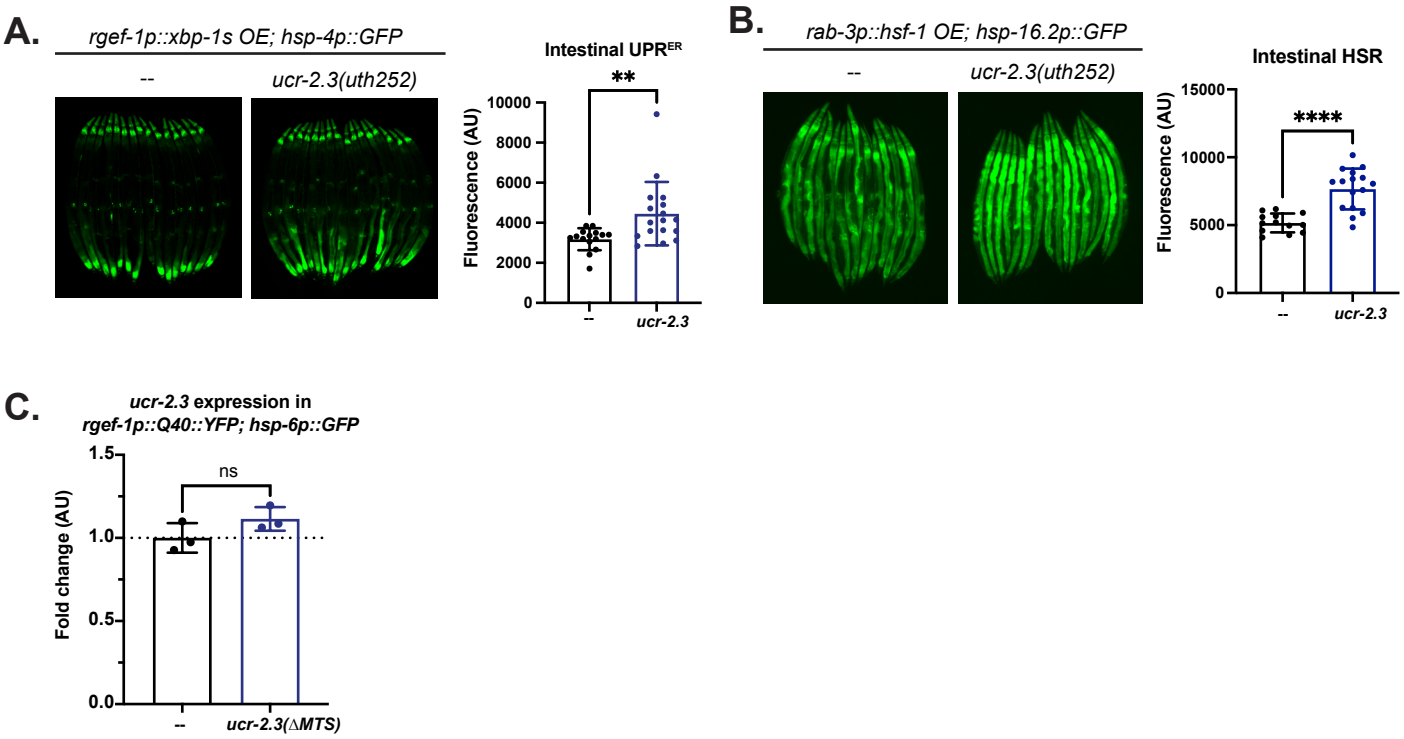

Supplemental Figure 3

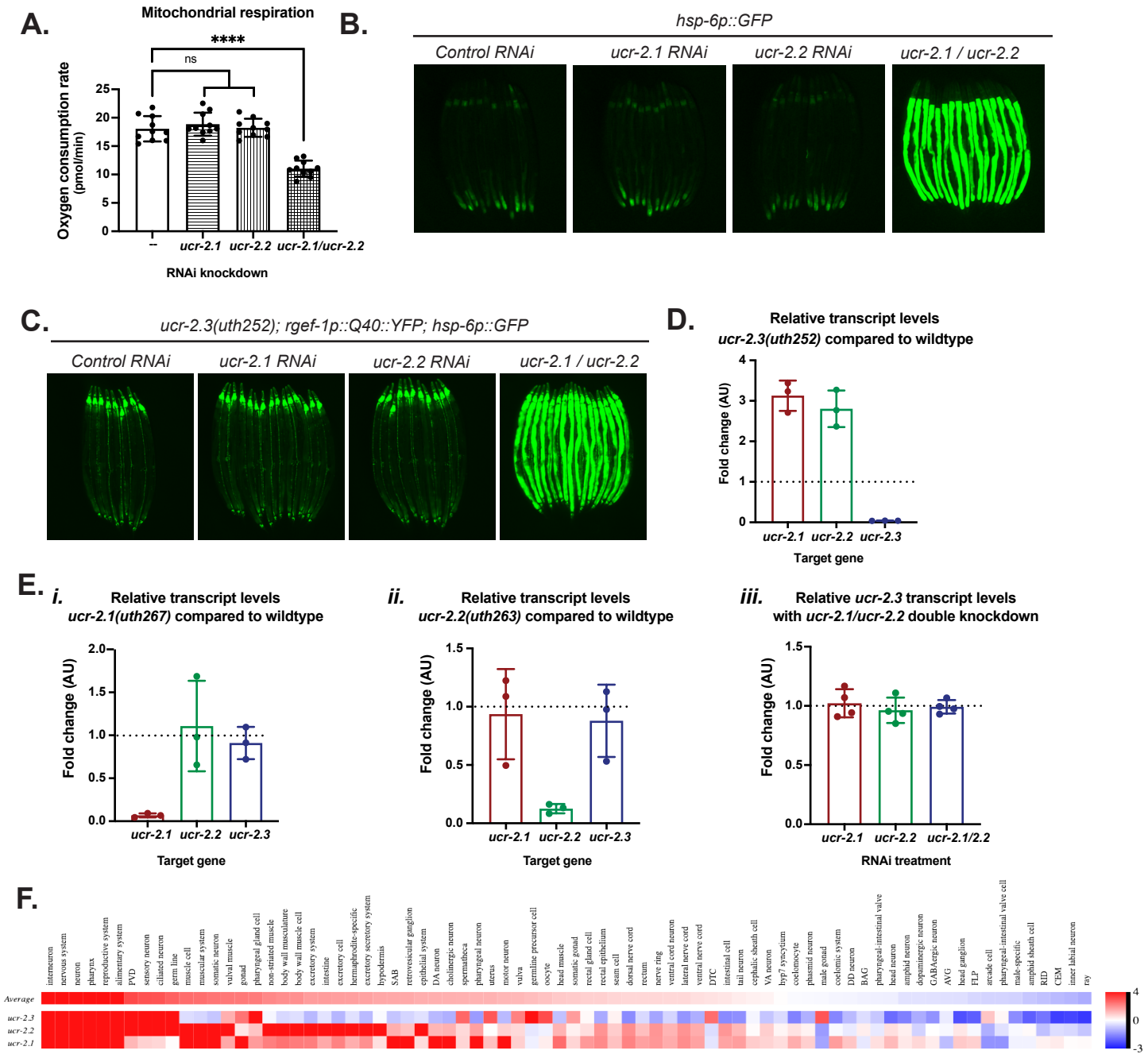

Supplementary Figure 4

A. ***i.***

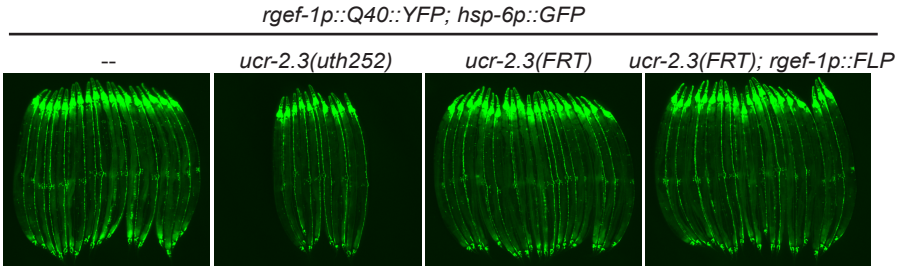

ii.

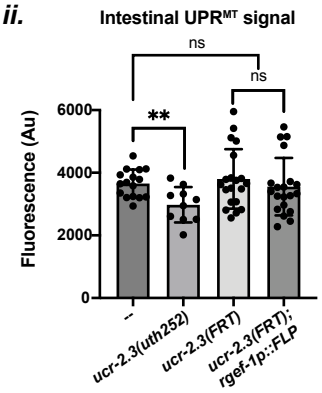

iii.

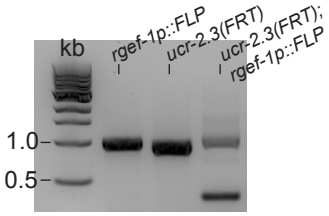

PCR product at *ucr-2.3* genomic locus

Supplementary Figure 5

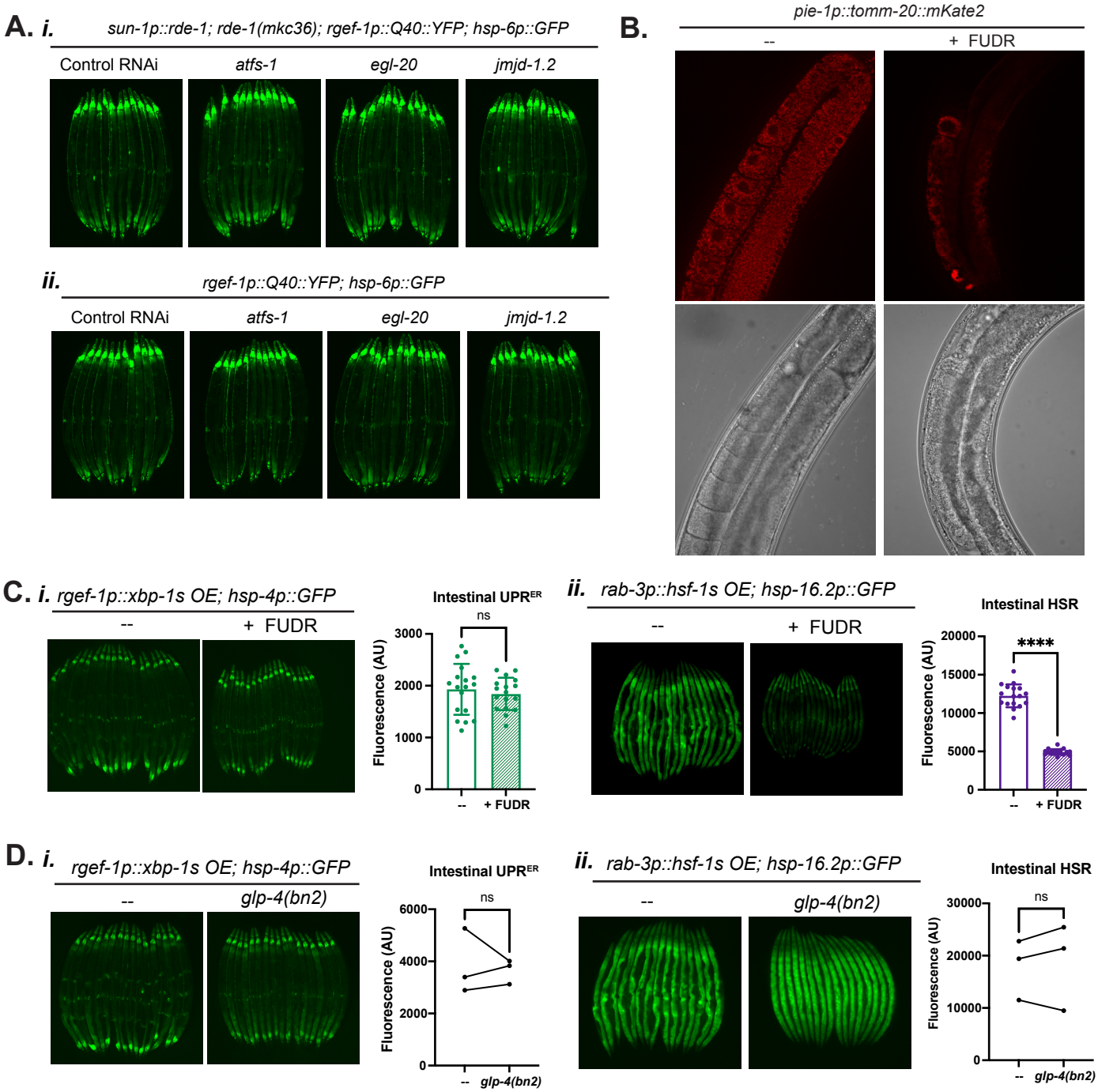

Supplemental Figure 6
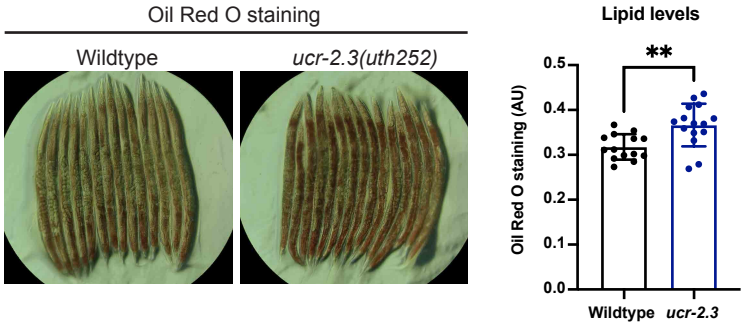
A.